BSJ

UIC Bioengineering Student Journal

Spring 2020 Volume X Issue 2

BSJ

University of Illinois at Chicago Bioengineering Student Journal

Spring
2020
Vol. X No.2

UIC Bioengineering Student Journal
Spring 2020
Volume X, No.2

Contents

Foreword

On behalf of the Department of Bioengineering, I am happy to present the second issue of the tenth volume of the UIC Bioengineering Student Journal. This journal continues to strive to provide both graduate and undergraduate students an opportunity to gain experience writing research articles for an academic publication. This is a great opportunity for students to take the knowledge and skills learned in their coursework and research and apply it to write a paper relevant to the field of bioengineering. Students who participate in this student-led journal go through a rigorous review process in which students receive multiple peer-reviews and go through several rounds of editing until receiving final approval from the editorial board. As a result, students can improve their technical writing skills as well as their intercommunication skills, which will benefit them in their future careers.

I would like to thank our Faculty Advisor, Dr. Magin for his continuous support in helping us organize and further develop the journal. Also, I would like to thank our Department Head Dr. Royston for continually supporting the journal's financial and logistical needs and allowing us to host release parties every year. Lastly, I would like to thank and congratulate the authors, reviewers, and editors who consistently put their best effort forward to contribute to the completion and success of both issues of this year's journal even in this unprecedented time.

Anupriya Mathews
Editor-In-Chief
Volume X, Issue 1

Editor-In-Chief
Volume X, Issue 2

THE GROWTH AND BENEFITS OF SONOGENETICS

Ameera Lodhi

alodhi7@uic.edu

Abstract

Sonogenetics explores the use of ultrasound in neuromodulation, as ultrasound waves are capable of exciting ion channels and subsequently exciting those neurons. This is proven in the vast literature which shows the targeting of genes in the model organism C. elegans. Sonogenetics also extends to genetic therapies tested on rats, including strengthening the expression of dopaminergic neurons in rats with Parkinson's, as well as the suppression of epilepsy. This noninvasive method is an improvement to treating Parkinson's symptoms with magnetic resonance-guided focused ultrasound pallidotomy (neurosurgical procedure whereby a tiny electrical probe is placed in the globus pallidus one of the basal nuclei of the brain which is then heated to 80 °C for 60 seconds, to destroy a small area of brain cells) , though the results of the MR-guided(Magnetic Resonance-Guided) focused ultrasound (MRgFUS) guided pallidotomy are beneficial in that indicate successful treatment in terms of patient motor function and quality of life. While there are risks associated with these experimental treatments, the promising results have made it a growing therapy option with numerous applications currently being implemented or explored.

Keywords: *Sonogenetics, focused ultrasound, blood-brain barrier, Parkinson's disease, Pallidotomy*

1. Introduction

Ultrasonic imaging is currently the most commonly practiced diagnostic procedure [7]. During an ultrasound, sound waves are emitted by a transducer, travel through tissue, and are scattered. Light, on the other hand, is unable to travel through tissue and therefore unusable for image reconstruction. Additionally, ultrasound provides a high temporal resolution. It can also be effectively coupled to multiple biological phenomena for potential illustration of physical interactions.

There are several limitations of ultrasonic imaging as well. Specifically, spatial precision is low for frequencies that are not highly attenuated by tissue. For this reason, magnetic resonance (MR) and X-ray can better penetrate bony areas and air-filled compartments. Over the years, ultrasound has grown in its imaging capabilities, and has been discovered as a promising treatment option for such disorders as Parkinson's disease (PD) [5,7]. The latest discovery is its ability to excite ion channels, and the subsequent research contributes to the growing field of sonogenetics [10].

2. Ultrasound Developments

Ultrasound as a diagnostic tool has grown due to the consistent improvements surrounding this technique.

2.1 Functional Ultrasound

Functional ultrasound (fUS) is one of the most immediately useful developments, being capable of enhanced sensitivity with neuroimaging [1]. Ultrafast ultrasound has much higher resolution, and faster image acquisition. When ultrafast ultrasound is combined with neurovascular coupling, it can be used to detect neural activity. This application has also been extended to ablation of targets within deep tissue [7].

2.2 Biomolecular Contrast Agents

The use of biomolecular contrast agents is another development within ultrasound [7]. Initially, bubbles were used as contrast agents due to their ability to bind with targets in the bloodstream. However, they have high Laplace pressure, are unstable in vivo, and cannot be used for the molecular imaging of active cellular processes.

Gas vesicles, which are found in bacteria and archaea, have a unique property in that they remain stable with their surroundings, achieving and maintaining equilibrium within microseconds.

Another property is that they collapse at specific acoustic pressures. The pressure at which the buckling occurs is dependent on the gas vesicle type, providing a wide, attainable range. Additionally, the gas vesicle does not collapse fully, and is compressible at specific frequencies [7]. This makes the buckling a reversible effect which can be manipulated through genetic engineering. They are especially detectable by ultrasound and are therefore effective acoustic reporter genes (ARGs).

2.3 Amplitude Modulation

Amplitude modulation increases contrast and specificity through the transmission of pulses above and below the buckling threshold. It is effective in vitro and in vivo.

3. Ultrasonic Treatment Developments

Improvements to the imaging capability of ultrasound were paired with ultrasonic treatment options. Today, ultrasound is a regularly utilized treatment for chronic pain through the application of heat, and there are countless studies on other potential therapies it can be used for [3].

3.1 High-Intensity Focused Ultrasound

High-intensity focused ultrasound (HIFU) uses acoustic focus for the ablation of tumors. This method has been used in China since the 1990s, and these capabilities have been known and investigated since the 1940s [4]. A study by Illing et al. tests the effectiveness of this method on liver and kidney tumors and evaluates the symptoms of the subjects.

The results of this study had a 100% success in liver tumor ablation and 67% success in kidney tumor ablation, as shown in Table 1. The symptoms were acute, including low-grade fever, mild discomfort, and skin toxicity which was spontaneously reversed. This method had significantly less impactful, and much fewer, adverse effects than invasive alternatives.

Table 1. HIFU Trial Results [4].

	Ablation seen in
Liver	
Radiologically assessed	20/20 (100%)
Histologically assessed	6/6 (100%)
Kidney	
Radiologically assessed	4/6 (67%)
Histologically assessed	1/4 (25%)

3.2 Treatment of Parkinson's Disease Through Pallidotomy

Pallidotomy is a current method of Parkinson's treatment utilizing extreme temperatures to scar affected regions of the brain. Pallidal lesioning is intended to improve motor function and control dyskinesia, or involuntary muscle movement associated with PD. Studies have found that it can be improved with the inclusion of MR-guided focused ultrasound (MRgFUS) [5]. The results of this investigation are shown in Figure 1.

When assessing long-term risk associated with MRgFUS pallidotomy, the investigators assessed patients after 1 year. This follow up suggested no side effects or complications. However, the procedure itself is associated with risk. For instance, there is the possibility of bleeding with a temperature increase beyond threshold temperature. It could also cause acute neurological damage. Additionally, there is a possibility of minimal improvement, as was the case for some patients. Nonetheless, this invasive treatment is practiced with and without the use of MRgFUS.
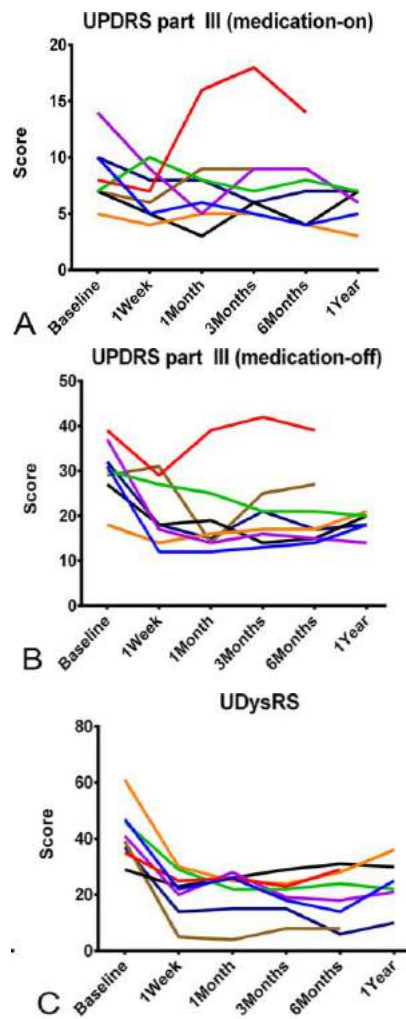
UPDRS part III (medication-on)

UPDRS part III (medication-off)

UDysRS

Figure 1. visualizes the Unified Parkinson's Disease Rating Scale (UPDRS) and Unified Dyskinesia Rating Scale (UDysRS) scores following MRgFUS pallidotomy. Each line represents a single patient. Based on these results, a majority of patients' quality of life improved at patients' 6 month and 12-month follow-ups, specifically with a 32.2%, then a 39.1% improvement in the Unified Parkinson's Disease Rating Scale and 52.7%, then 42.7% improvement in Unified Dyskinesia Rating Scale. There was more reliable improvement in "medication-off," or non-medication-induced dyskinesia [5].

3. Background of Sonogenetics

The desire to monitor and control neural activity has existed for decades, and numerous methods have been investigated [7]. Optogenetics is an invasive option, requiring the insertion of fiber optics due to the inability of light wavelengths to reach deep tissue [3].

On the other hand, ultrasound can cause the expression of ion channels. Its excitatory properties have been known and investigated for more than 80 years [6]. It was first found to express ion channels through temperature changes. In 2008, it was revealed that when it applies pressure to mechanosensitive ion channels, the mechanical strain leads to an increase in membrane tension [10]. Due to the tension-dependent gating of these channels, they are then activated. This is now the growing field of sonogenetics, with its growth shown in Figure 2.
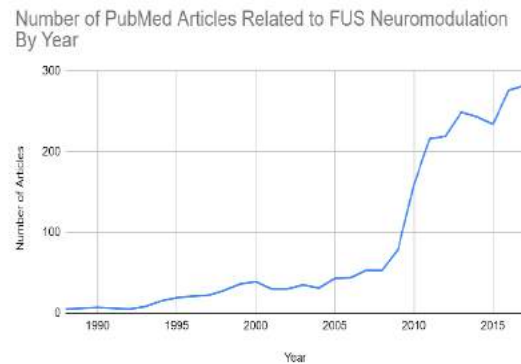

Figure 2. Number of articles on ultrasound and gene expression or neuromodulation published on PubMed from 1988 – 2018.

This phenomenon has been tested on the model organism *C. elegans*, which have an advanced nervous system, and can indicate changes in neural activity through their locomotion [3]. TRP-4 channels were specifically targeted due to their sensitivity to low-pressure ultrasound. These channels would not be damaged, nor would there be detectable change in temperature, accounting for those potential confounding variables. Subsequent changes in behavior and locomotion were observed for. Organisms lacking a TRP-4 channel lacked notable responses to peak stimulation pressures, confirming the successful stimulation. These effects were amplified when used with microbubbles, with smaller microbubbles causing larger amplification.

4. Therapy Implications

The ability of ultrasound to express central and peripheral neurons and nerves was extended to

therapies for epilepsy, Parkinson's, and, as explored previously, pain treatment.

4.1 Epilepsy

Focused ultrasound has been found to suppress epileptic activity in rats using neuromodulation [9]. In a study by Min et. al., an acoustic wave of mechanical index below that which would disrupt the blood-brain barrier (BBB) was applied with microbubbles in order to activate voltage-gated sodium/calcium channels and subsequently manipulate brain activity and neurotransmission. Brain activity was monitored by EEG during induced epileptic episodes. Behavior and body weight were monitored during the two-week experiment.

After detecting an epileptic signal in rats, FUS was applied to one of two experimental groups. This group exhibited significantly fewer electroencephalography (EEG) signal bursts than the untreated group. They were also shorter in duration. A second sonication, again, reduced them further. Behaviorally, while both groups recovered, the FUS-treated group was less convulsive during episodes. Both groups also had similar long-term results.

The safety of FUS was also evaluated in this study, and it was determined that there were no instances of damage to targeted tissue or cells. Therefore, FUS was deemed a promising therapy for epilepsy. The researchers also claim that its properties can be extended to neurological and psychological conditions including chronic pain, movement disorders, post-traumatic stress disorder, and depression.

4.2 Parkinson's Disease

Another implication of the excitatory capabilities of ultrasound is the non-invasive expression of dopamine in patients with Parkinson's disease (PD). As was mentioned earlier, patients with Parkinson's Disease have degenerated dopaminergic neurons. They subsequently present with bradykinesia, rigidity, and tremors. This method has recently been approved by the FDA for the Parkinson's disease symptoms of tremor and dyskinesia.

MR image-guided FUS can also open the blood-brain barrier [8]. However, instead of treating through invasive pallidotomy, focused ultrasound is applied in order to open the blood-brain barrier and noninvasively deliver a neurotrophic factor for its expression, as displayed in Figure 3.While not related to the expression of a gene by tension-dependence, this method uses FUS manipulates of brain cells and open the BBB in order to deliver glial cell-line derived neurotrophic factor (GDNF) to the brain, which will cause GDNF transgene expression.

Mead et. al. tested this method on rats [8]. MR image-guided FUS was coupled with brain-penetrating nanoparticles to express glia, allowing for targeted gene expression. Treatment through targeted FUS successfully restored dopamine levels and dopaminergic neuron density in the rats. This corresponded with symptomatic improvement in rats' locomotor function, which was also scored. It was concluded that successful GDNF expression greatly improved PD-associated motor dysfunction.
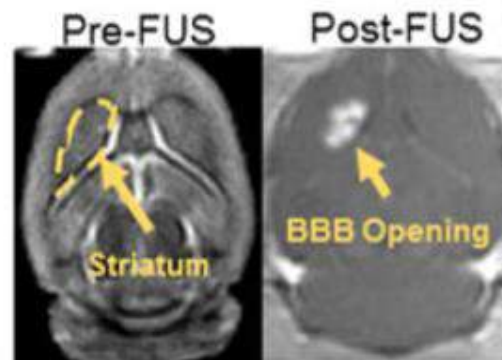
Figure 3. Noninvasive opening of the blood-brain barrier when FUS is applied in the targeted area with microbubbles [7].

The repeated blood-brain barrier opening is, however, a safety concern [2]. The associated risk was assessed in 2014 by Downs et. al., which studied the repeated opening of the BBB with FUS with microbubbles on 4 primates. They opened the BBB of 4 basal ganglia regions responsible for voluntary motor control, memory, and other functions affected by Parkinson's disease.

Vital signs were monitored to observe physiological changes during the BBB opening and T1-weighted MRI was used to validate successful opening of the BBB. To assess safety, T2-weighted and susceptibility-weighted image (SWI) MRI scans were done to analyze cellular health during and after BBB opening. Secondly, behavioral observation and testing accounted for changes in neurological function. Qualitative behavioral testing accounted for movement, eating, drinking, and socialization.

Vital signs remained stable during the procedure, and successful BBB opening was verified 98% of the time. Based on T2 and SWI scans, no hemorrhage or edema was observed. There were 4 cases of possible edema during final FUS which were untraceable 1 week later and thus self-resolved. This result is shown in Figure 4. There were no qualitative changes in the assessed behavior, and the effects on behavioral testing were minimal and non-permanent.
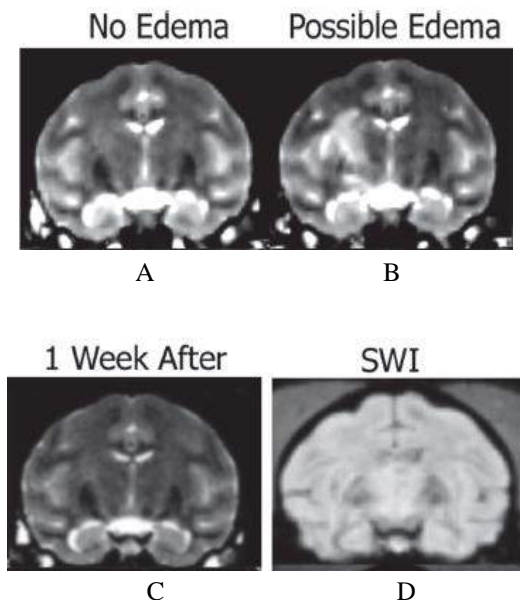

Figure 4. The evaluation of edema using T2-weighted sequences. A. Scan with no edema. B. A scan containing a hyperintense target region with a possible edema. C. No edema, as in A, indicating a reversal from the previous week. D. Scan taken the same day as B, showing the second SWI scan with a possible edema [2].

6. Conclusion

Ultrasound neuromodulation has been shown to be an effective, low-risk, noninvasive method of treatment for epilepsy and Parkinson's symptoms. When compared to even other ultrasound developments, this is more promising than invasive procedures currently in practice, such as pallidotomy.

While HIFU has been in practice for decades, HIFU devices have yet to be expanded to the West. Similarly, before the implementation of focused low-frequency ultrasound is either not yet approved or has been recently approved. Although there has been dense research done on the same in the recent years, there must be further investigation in the coming years as well.

5. References

1. Deffieux, T., Demene, C., Pernot, M., Tanter, M. Functional ultrasound neuroimaging: a review of the preclinical and clinical state of the art. *Current Opinion in Neurobiology*. 50:128-135, 2018.

2. Downs, M. E., Buch, A., Sierra, C., Karakatsani, M. E., Teichert, T., Chen, S., … Ferrera, V. P. Long-Term Safety of Repeated Blood-Brain Barrier Opening via Focused Ultrasound with Microbubbles in Non-Human Primates Performing a Cognitive Task. *PLoS one*. 10:5, 2015.

3. Ibsen, S. Sonogenetics is a non-invasive approach to activating neurons in Caenorhabditis elegans. *Nature Communications*. 6, 2015.

4. Illing, R. O., Kennedy, J. E., Wu, F., ter Haar, G. R., Protheroe, A. S., Friend, P. J., Middleton, M. R. The safety and feasibility of extracorporeal high-intensity focused ultrasound (HIFU) for the treatment of liver and kidney tumors in a Western population. *British Journal of Cancer*. 93:890–895, 2005.

5. Jung, N. Y. The efficacy and limits of magnetic resonance–guided focused ultrasound pallidotomy for Parkinson's disease: A Phase I clinical trial. *Journal of Neurosurgery*. 130:1853–1861, 2019.

6. Kubanek, J. Ultrasound Elicits Behavioral Responses through Mechanical Effects on Neurons and Ion Channels in a Simple Nervous System. *Journal of Neuroscience Research*. 38:12, 2018.

7. Maresca D, Lakshmanan A, Abedi M, et al. (2018). Biomolecular Ultrasound and Sonogenetics. *Annual Review of Chemical and Biomolecular Engineering*. 9:229–252, 2018.

8. Mead, B. P. Novel Focused Ultrasound Gene Therapy Approach Noninvasively Restores Dopaminergic Neuron Function in a Rat Parkinson's Disease Model. *Nano Letters*. 17:6, 2017.

9. Min, B.-K., Bystritsky, A., Jung, K.-I., Fischer, K., Zhang, Y., Maeng, L.-S., … Yoo, S.-S. Focused ultrasound-mediated suppression of chemically induced acute epileptic EEG activity. *BMC Neuroscience*. 12 :23, 2011.

10. Tyler, W.J., Tufail, Y., Finsterwald, M., Tauchmann, M.L., Olson, E.J., Majestic, C. Remote Excitation of Neuronal Circuits Using Low-Intensity, Low-Frequency Ultrasound. *PLoS ONE*. 3:10, 2008.

MICROBUBBLES AS CONTRAST ENHANCEMENT IN ULTRASOUND IMAGING FOR PATHOPHYSIOLOGY DETECTION AND IMAGE-GUIDED THERAPIES

Celine Macaraniag

cmacar3@uic.edu

Abstract

Ultrasound imaging is a non-invasive, dynamic method to image biological tissues and blood vessels. This imaging modality is highly desirable compared to others that involve ionizing radiation which may lead to adverse health effects. The ability to image microvasculature is imperative for the early detection of pathophysiology and for the ability to guide drug-delivery and/or gene-therapy. However, microvasculature imaging can be difficult to achieve using conventional techniques due to limitations in resolution. To achieve high-resolution imaging in the microscale, microbubbles are introduced as contrast enhancements for ultrasound. These microbubbles can be controlled in size and stability. This technique, also known as contrast-enhanced ultrasound (CEUS), has been shown to detect pathophysiology in the microvasculature, about 10-70 μm in diameter, not easily resolved with other conventional techniques. Imaging in the microscale can also provide fundamental insights in diseases such as coronary arterial disease, peripheral vascular disease, type II diabetes, myocarditis, etc. For instance, muscle glucose is dependent on insulin activity on the endothelium of skeletal muscle microvasculature. Patients with diabetes have impaired insulin activity, therefore, it is advantageous to study their microvascular response to insulin thus providing crucial information about disease progression. In addition, CEUS can also be used in guiding drug-delivery strategies since it is capable of tissue and vessel localization. Current research is moving towards optimizing this technique to ultimately be able to provide high resolution in vivo imaging. In this review article, first, the mechanism behind microbubble contrast enhancements will be discussed. Second, different approaches of CEUS imaging for biomedical applications will be listed and compared, specifically, for cardiovascular diagnostics, image guided cancer therapy, drug delivery, and gene therapy. And lastly, current limitations to the technology will be reviewed. This article will hopefully provide insight into how CEUS technology may advance cardiovascular medicine and cancer therapy given its diagnostic and therapeutic utility.

Keywords: *Ultrasound, contrast-enhanced ultrasound, microbubbles, microvascular imaging, ultrasound-guided therapy*

1. Introduction

Ultrasound imaging is a non-invasive, dynamic method to visualize biological tissues and vasculature. Other imaging modalities that offer remarkably high sensitivity such as single photon emission computed tomography (SPECT) and positron emission tomography (PET) use ionizing radiation which can have detrimental health effects, especially after repeated and long exposure. These modalities cannot be used for frequent and long-term monitoring [13]. Although magnetic resonance imaging (MRI) offers significantly high spatial resolution, it is contraindicated with implanted material and thus may not be used in patients with intra-cardiac devices [13]. Ultrasound imaging, in addition to its non-invasive nature, holds adequate sensitivity and spatial

resolution without having to use ionizing radiation and other potentially toxic agents [13]. Contrast-enhanced ultrasound (CEUS) can achieve super-resolution visualization of micro vessels with the use of engineered gas-filled microbubbles (~1 to 8 μm in diameter) as contrast agents. Image resolution of ultrasound is significantly enhanced with these contrast agents. Tiny blood vessels ~10-70 μm in diameter [3,5] can now be visualized with ultrasound as microbubbles flow through the vessels. Without contrast enhancements, blood vessels are hard to resolve since they reflect sound poorly making them difficult to visualize. Gas-filled microbubbles address this limitation since they are able to scatter sound very well and therefore are good point sources [2].

Advancements in high-resolution medical imaging offer early detection of pathophysiology in vascular structures. Abnormalities in micro-vessels may be assessed whether they partly cause or lead to arterial disease [10]. Additionally, therapy through drug- or gene-delivery may be studied through imaging in real time to monitor drug-transport without any invasive procedures [15]. In this review, mechanisms behind microbubble ultrasound imaging will be discussed. Then, several approaches to CEUS imaging for biomedical applications will be listed and compared, specifically in vascular disease diagnostics, image guided cancer therapy, drug delivery, and gene therapy. And lastly, current limitations and future directions to the technology will be reviewed.

2. Physical Mechanism of Microbubbles as Contrast Agents in CEUS

Ultrasound transducers emit sound waves that vary acoustic pressure. Acoustic signals are generated from the backscattering of sound with frequencies greater than 20 kHz beyond the range of what humans can hear [10]. The benefit of using microbubbles as contrast enhancements in ultrasound imaging is that they are able to expand and compress easily. Microbubbles undergo resonant volumetric oscillations due to the changes in pressures leading to asymmetric changes in microbubble diameter [10]. Compressions happen along with pressure peaks, and expansions happen along with pressure nadirs. The vibration of these agents in the ultrasound field generates strong backscattered signals [10]. The Rayleigh-Plesset equation describes the dynamic microbubble response to an ultrasonic field [8]. Equation (1) is the linearization of the Rayleigh-Plesset equation resembling a mass-spring system where gas is the spring and the surrounding liquid is the mass [12].

$$\ddot{x} + 2z\omega_0\dot{x} + \omega_0{}^2 x = \frac{p_A}{\rho R_0} sin\ \omega t \qquad (1)$$

In the above equation,
- x represents the variation in the radius, R, of the microbubble
- $\dot{x}$ and $\ddot{x}$ are the 1st and 2nd derivatives of x
- z is the damping of the system
- ω_0 is the bubble oscillation eigenfrequency
- p_A is the driving pressure amplitude

- ρ is the density of the liquid
- R_0 is the equilibrium radius
- ω represents the angular ultrasound frequency

Microbubbles oscillate in maximum amplitude in response to ultrasound pulse. The oscillation is due to the resistance against compression of gas inside and the inertia of the liquid in the surroundings [12]. It is important to closely match incoming ultrasound frequency with resonance frequency as much as possible to maximize acoustic response. Overtime, this system will experience damping due to energy dissipation in the surrounding fluid, reradiation of sound, and thermal energy loss [12]. Figure 1A shows that microbubbles of different sizes have varying maximum amplitude of oscillation and that in smaller bubbles damping increases. In different acoustic pressures, below 50 kPa, the radius of maximal response changes, but when the acoustic pressure exceeds 50 kPa, the radius response remains the same. This phenomena is due to the resonance frequency no longer being influenced by the characteristics of the bubble shell [12]. The maximum oscillation amplitudes occur when the ultrasound frequency matches the resonance frequency. Further, physicochemical properties (i.e. lipid coating and influence of nearby structures) also contribute to the alteration of resonance of the bubble [12].
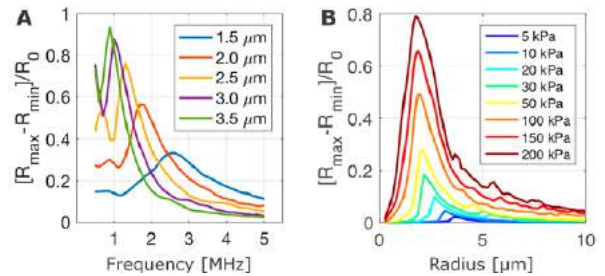

Figure 1. Relative oscillation amplitudes of a bubble. (A) Variations in frequency and microbubble size, where different sizes have varying maximum amplitude of oscillation. (B) Variations in microbubble size and acoustic pressure at 2 MHz ultrasound frequency. At above 50 kPa, the radius of response remains the same [12].

The composition of microbubble agents are gases which are non-toxic and have low solubility to blood [7]. Gases most commonly used in microbubbles are: octafluoro propane (C3F8), deca-fluoro butane (C4F10) and sulfur hexafluoride (SF6) [7]. The mean diameter range of microbubbles is around 1-4 μm [7], microscopic image shown in Figure 2.
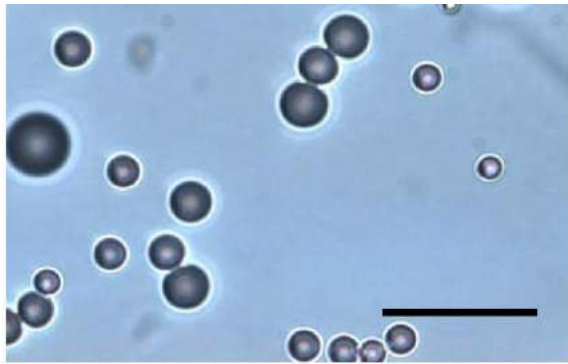
Figure 2. Microbubble preparation imaged under a microscope. Scale bar, 10 μm [7].

Encapsulation of the microbubble within a protective shell further maintains the stability of microbubbles in vivo. Materials such as lipids, biopolymers like polyethylene glycol (PEG), other ligands, and proteins [13] have all been used in shells that encapsulate these contrast agents to ensure their potency and localization within the tissues or vessels [4]. Not only does encapsulation prolong the viability of microbubbles, but it also presents a way for drugs to be loaded onto the shell. Figure 3 shows an example of a microbubble encapsulated in a polymer and albumin shell loaded with Doxorubicin drug. This capability opens an avenue for drug and gene delivery which will be reviewed further in a later section of this article. Though, careful consideration must be taken when designing microbubbles and their shells so that its acoustic damping does not heavily interfere with the volumetric oscillations of the bubbles [7].
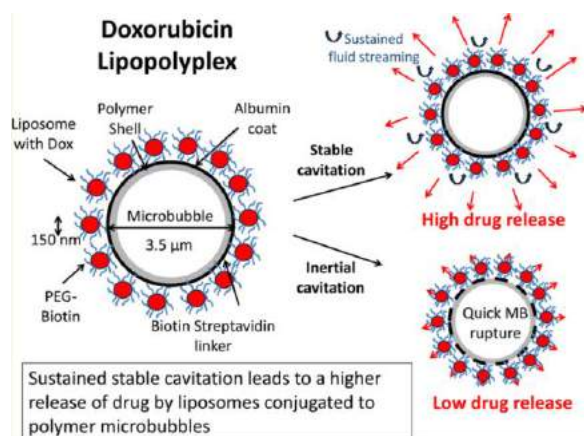

Figure 3. Schematic diagram of a microbubble encapsulated with polymer and albumin shell conjugated with PEG biotin and Doxorubicin liposome [16].

When imaging specific tissues, it is important to target microbubbles that are representative of the tissue one wants to image. There are two strategies in which this is done: (1) using the chemical or electrostatic properties of the microbubble shell that help microbubbles stay within the diseased tissues, and (2) using antibodies, peptides, or other ligands attached to the surface of microbubbles that recognize disease-related antigens [10]. To differentiate between these target microbubbles from freely circulating ones, a common protocol is followed. The graph shown in Figure 4 illustrates this protocol: (1) most of the signal from tissue in interval A, right after administration of a targeted agent, will be from freely moving agents; (2) the microbubble accumulates at the target when the concentration is high in interval B; and lastly, (3) late signal enhancement in interval C occurs after clearance of freely circulating microbubbles which then represents the target signal [9].
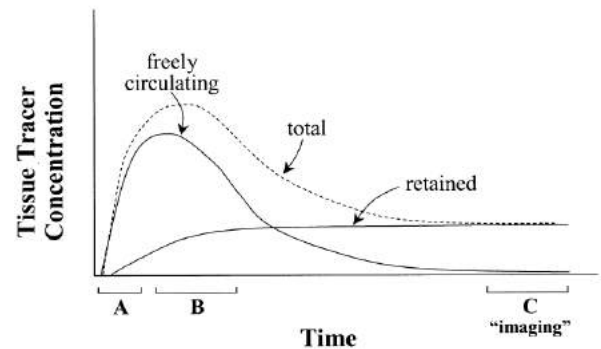

Figure 4. Tracer concentration over time. A, B, and C refer to intervals where signals represent different tracer activities. In interval C, clearance of freely circulating microbubbles occurs and acquired signal represents the desired signal [9].

3. Biomedical Applications

Imaging in the microscale can provide fundamental insights into many vascular-related diseases such as coronary arterial disease, peripheral vascular disease, type II diabetes, myocarditis, etc. For instance, muscle glucose is dependent on insulin activity on the endothelium of skeletal muscle microvasculature. Patients with diabetes have impaired insulin activity and therefore it is advantageous to study their microvascular response to insulin thus providing important information about disease progression. Strategies to combat these diseases as much as possible are important to develop and optimize. CEUS offers promising directions in biomedical imaging,

diagnostics, and treatment with its ability to visualize in the microscale.

3.1 Microvascular Imaging

A 2015 study by Christensen-Jeffries et al. [1] demonstrated a super-resolution imaging of microvasculature visualizing 19 μm vessels and blood flow velocity using single bubble localization. This ability to acquire flow velocity information in high resolution presents great promise in the advancement of imaging for diagnosis and monitoring of diseases. Many other physiological and pathological processes may be studied with the use of CEUS such as neovascularization, early stage ischemia, and tumor growth [1].

Errico et al. [3] also demonstrated super-resolution ultrasound imaging of rat brain microvasculature by capturing the transient signal decorrelation of microbubbles achieving hemodynamic quantification of cerebral microvasculature (about <10 μm in diameter) that was more than 10 mm below the tissue's surface [3]. By tracking microbubble movement through the vessels, they were able to obtain instantaneous position of in-plane velocity and therefore local cerebral blood velocity [3]. Advancements in resolution have also been demonstrated in a recent study conducted by Yu et. al. [17], where they performed in vivo CEUS imaging of rabbit ear microvasculature with a diameter of 41 μm, remarkably improving temporal resolution using a deconvolution technique [17]. High-resolution imaging enables the study of many areas of biomedical research including new formation of vessels from pre-existing vasculature, a process called angiogenesis. Angiogenesis is a necessary process involved in the proper perfusion of tissues. Thus, it is important to consider this process when investigating ischemia that emanates from coronary and peripheral vascular diseases [13]. It is possible to monitor the process of angiogenesis through CEUS since microbubbles remain completely intravascular [13], therefore offering selective imaging of the target vasculature.

3.2 Vascular Disease Diagnosis

Cardiovascular disease is the leading cause of death in the United States according to the Center of Disease Control and Prevention [18]. Thus, it is imperative to detect pathologies early so that physicians can plan treatment effectively and ultimately decrease mortality rates. Many strategies to diagnose cardiovascular disease exist but one very important advancement is CEUS for microvascular imaging. The diagnostic and therapeutic potential of CEUS imaging has already emerged in carotid arterial disease, aortic disease, and peripheral arterial disease [13]. CEUS has shown to perform better than conventional ultrasound imaging in terms of resolution and diagnostic efficacy [4]. It is able to identify vessel abnormalities, quantify neovascularization in atherosclerotic plaques, and assess end-muscle perfusion [11]. The emerging technology of microbubbles and CEUS imaging holds considerable promise for cardiovascular medicine and cancer therapy given its diagnostic and therapeutic utility [11]. Researchers are also taking advantage of CEUS to study disease progression. A recent study by Ghosh et al. showed successful CEUS imaging of microvascular recruitment. They studied vascularization in response to insulin in the murine skeletal muscle. Although their study was performed in anesthetized animals, they observed vascular recruitment after insulin infusion [5]. Further study of this strategy with improved experimental conditions may provide even stronger evidence of the efficacy of the diagnostic capability of CEUS.

3.3 Ultrasound-guided Gene Therapy

Several other applications may be performed with microbubble ultrasound. Microbubbles as agents in therapeutic applications have been demonstrated in targeted drug delivery and gene therapy as well as for sonothrombolysis enhancement [11]. Ultrasound-aided gene delivery modifies the microbubble technique to perform gene delivery. Microbubbles are loaded with plasmids and are intravenously injected. Monitoring gene-delivery with ultrasound imaging would provide real-time feedback about the status of the therapy to clinicians [13]. Drugs may be loaded onto the microbubble shell directly and their release may be triggered by ultrasound at a desired time and location for precise targeting [12]. This localized method of delivery prevents side effects of high concentrations of drugs in chemotherapy or anti-inflammatory therapies [12]. Figure 5 depicts the process in which a microbubble may deliver materials to the cell [6].
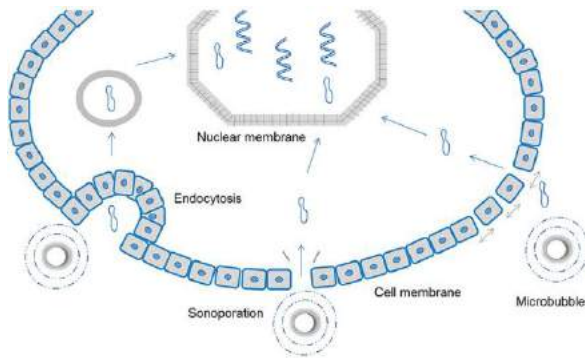
Figure 5. Schematic of ultrasound–guided gene delivery using microbubbles [6].

3.4   Applications in Cancer Therapy

Cancer therapy usually requires aid from imaging to find lesions in tissues with tumors. For instance, neoadjuvant chemotherapy (NAC) is a standard treatment for patients with locally advanced breast cancers. It is important to identify pathological response in breast cancer patients receiving chemotherapy [14]. Recently, a study on chemotherapy in a tumor model was performed with CEUS imaging. Xiao et al. [15] showed improved drug delivery with low-frequency ultrasound the presence of microbubbles and demonstrated minimization of adverse effects to surrounding normal tissues. Low-frequency microbubble ultrasound caused changes in the interstitial fluid pressure (IFP) and therefore improved Doxorubicin penetration in a virus-induced rabbit carcinoma model (VX2 tumor) [15]. This mechanical alteration using ultrasound show a potential new strategy to improve chemotherapy effects.

4. Summary and Future Directions

CEUS is an attractive method for imaging biological tissues and vessels since it is non-invasive and able to image in real time. Ultrasound-microbubble imaging can detect micro-vessel activity including insulin response, pathophysiology, and drug/gene delivery. Additional research studies are needed for CEUS technology to be translated to practical use in biomedical research, clinical diagnostics, and drug-delivery means. Large sample sizes are required for further experiments to advance this technology into clinical practice [11]. Early clinical trials need to be thoroughly designed as well [13]. In gene-delivery, angiogenic growth factor genes, gene combinations, and timing of delivery need to be further researched

[13]. The ability to image microvasculature offers great potential in detecting pathophysiology and guiding drug delivery. Optimization of this technique is important in order to improve resolution for visualizing even the smallest of vessels with diameters in the order of micrometers. Furthermore, integration of cancer- and gene-therapy with CEUS imaging is an encouraging direction for new therapeutic strategies. Ongoing research is underway to address these issues to further improve this technique to provide more accurate diagnostics and highly sensitive therapies.

5. References

1. Christensen-Jeffries, K., R. J. Browning, M.-X. Tang, C. Dunsby, and R. J. Eckersley. In Vivo Acoustic Super-Resolution and Super-Resolved Velocity Mapping Using Microbubbles. *IEEE Transactions on Medical Imaging*. 34:433–440, 2015.

2. Cox, B., and P. Beard. Super-resolution ultrasound. *Nature*. 527:451–452, 2015.

3. Errico, C., J. Pierre, S. Pezet, Y. Desailly, Z. Lenkei, O. Couture, and M. Tanter. Ultrafast ultrasound localization microscopy for deep super-resolution vascular imaging. *Nature*.527:499–502, 2015.

4. Feinstein, S. B. The powerful microbubble: from bench to bedside, from intravascular indicator to therapeutic delivery system, and beyond. *American Journal of Physiology-Heart and Circulatory Physiology*. 287:H450–H457, 2004.

5. Ghosh, D., J. Peng, K. Brown, S. Sirsi, C. Mineo, P. W. Shaul, and K. Hoyt. Super-Resolution Ultrasound Imaging of Skeletal Muscle Microvascular Dysfunction in an Animal Model of Type 2 Diabetes. *Journal of Ultrasound in Medicine.* 38:2589–2599, 2019.

6. Huang, C., H. Zhang, and R. Bai. Advances in ultrasound-targeted microbubble-mediated gene therapy for liver fibrosis. *Acta Pharmaceutica Sinica B.* 7:447–452, 2017.

7. Juang, E. K., I. De Cock, C. Keravnou, M. K. Gallagher, S. B. Keller, Y. Zheng, and M. Averkiou. Engineered 3D Microvascular Networks for the Study of Ultrasound-Microbubble-Mediated Drug Delivery. *Langmuir*. 35:10128–10138, 2019.

8. Kaufmann, B. A. Ultrasound Molecular Imaging of Cardiovascular Disease. *Current Cardiovascular Imaging Reports.* 3:18–25, 2010.

9. Kokhuis, T. J. A., B. A. Naaijkens, L. J. M. Juffermans, O. Kamp, A. F. W. van der Steen, M. Versluis, and N. de Jong. On the dynamics of StemBells: Microbubble-conjugated stem cells for ultrasound-controlled delivery. *Applied Physics Letters.* 111:023701, 2017.

10. Kooiman, K., H. J. Vos, M. Versluis, and N. de Jong. Acoustic behavior of microbubbles and implications for drug delivery. *Advanced Drug Delivery Reviews.* 72:28–48, 2014.

11. Lindner, J. Molecular imaging with contrast ultrasound and targeted microbubbles. *Journal of Nuclear Cardiology.* 11:215–221, 2004.

12. Lindner, J. R. Microbubbles in medical imaging: current applications and future directions. *Nature Reviews Drug Discovery.* 3:527–533, 2004.

13. Mehta, K. S., J. J. Lee, A. A. Taha, E. Avgerinos, and R. A. Chaer. Vascular applications of contrast-enhanced ultrasound imaging. *Journal of Vascular Surgery*. 66:266–274, 2017.

14. Roovers, S., T. Segers, G. Lajoinie, J. Deprez, M. Versluis, S. C. De Smedt, and I. Lentacker. The Role of Ultrasound-Driven Microbubble Dynamics in Drug Delivery: From Microbubble Fundamentals to Clinical Translation. *Langmuir.* 35:10173–10191, 2019.

15. Smith, A. H., H. Fujii, M. A. Kuliszewski, and H. Leong-Poi. Contrast Ultrasound and Targeted Microbubbles: Diagnostic and Therapeutic Applications for Angiogenesis. *J. of Cardiovasc. Trans. Res.* 4:404–415, 2011.

16. Wan, C.-F., X.-S. Liu, L. Wang, J. Zhang, J.-S. Lu, and F.-H. Li. Quantitative contrast-enhanced ultrasound evaluation of pathological complete response in patients with locally advanced breast cancer receiving neoadjuvant chemotherapy. *European Journal of Radiology*.103:118–123, 2018.

17. Xiao, N., J. Liu, L. Liao, J. Sun, W. Jin, and X. Shu. Ultrasound Combined with Microbubbles Increase the Delivery of Doxorubicin by Reducing the Interstitial Fluid Pressure. *Ultrasound Quarterly* .35:103–109, 2019.

18. Yu, F. T. H., X. Chen, J. Wang, B. Qin, and F. S. Villanueva. Low Intensity Ultrasound Mediated Liposomal Doxorubicin Delivery Using Polymer Microbubbles. *Molecular Pharmaceutics.* 13:55–64, 2016.

19. Yu, J., L. Lavery, and K. Kim. Super-resolution ultrasound imaging method for microvasculature in vivo with a high temporal accuracy. *Scientific Reports.* 8:13918, 2018.

20. Know the Facts About Heart Disease at <https://www.cdc.gov/heartdisease/docs/ConsumerEd_HeartDisease.pdf>. Accessed November 5, 2019.

IMPROVING MR IMAGING BY ACOUSTIC NOISE REDUCTION: AN OVERVIEW OF METHODS USED FOR ACOUSTIC NOISE REDUCTION

Farhin Patel

fpatel29@uic.edu

Abstract

Acoustic noise in MRI poses a problem in patient scanning as well as in many areas of psychiatric and neuroscience research such as functional MRI. Some physical factors involved in hearing loss include the sound frequency, temporal pattern, and intensity of noise levels. High noise levels at low frequencies can cause temporary hearing loss which proves to be a hindrance in communication for both patients and professionals present. Changing the imaging parameters such as section thickness, field of view, repetition time, and echo time cause the noise level to vary. This paper reflects on the various ways the acoustic noise reduction is done. Acoustic noise can be decreased either by reducing noise sources or by blocking pathways carrying the noise to the region of interest. There are also passive ways to reduce the acoustic noise levels which helps in dampening the noise to a certain level.

Keywords*: Acoustic noise, MRI, magnetic field, current, rf coil, gradient noise, eddy current*

1. Introduction

Of all imaging techniques, ultrasound, and Magnetic Resonance Imaging (MRI) use non-ionizing radiation methods which prove to be a safer option compared to imaging methods dependent on ionizing radiation. MRI is more advantageous as it accommodates imaging of all body structures in all three planes. MR Imaging, although claustrophobic and time consuming, provides high resolution images of physical and chemical data. Acoustic noise is any sound in the acoustic domain. The acoustic noise in MRI is mainly caused by the gradient magnetic field, which is caused by the rapid alterations of current, causing vibrations within the gradient coils. These currents, in the presence of a strong static magnetic field of the MR system, produce significant forces that act upon the gradient coils. Noise levels in MRI have been reported to go higher than 130 decibels (dB) [8]. Noise that high in an enclosed space does not help the patient feel comfortable during an MRI scan.

2. Acoustic Noise Effects on fMRI

Functional MRI (fMRI) measures brain activity by detecting changes associated with blood flow. The brain is where most of the sensory activity occurs. Therefore, when a person is annoyed due to the acoustic noise levels, it is reflected in their fMRI imaging. This change in brain activity caused by acoustic noise can lead to inaccurate fMRI images which could lead to wrong diagnosis for the patient. The sound pressure levels (SPL) with mean reduction of SPL across the spectrum of 12 dB from standard to silent sequences was used to access the

effects of acoustic noise on fMRI [6]. The lower levels of acoustic noise promote stronger temporal coupling between RSNs (Resting State brain Networks) implicated the cognitive function and areas dedicated to reasoning, visceral self-monitoring and associative areas. The higher noise induced an overload in the DMN (default mode network), more specifically in the posterior cingulate cortex [7]. This shows the importance of acoustic noise reduction on fMRI.

To measure the acoustic noise levels in Magnetic Resonance Imaging, nonmagnetic microphone, wood and brass for fixation must be used due to the high magnetic fields in and around the MR system. The microphone is omnidirectional microphone of electret condenser microphone (ECM). The vibrating membrane is polyester, the back electrode is brass. It also has a field effect transistor (FET) and the cover is made of aluminum and resin [1]. The equation for calculating continuous A-weighted sound pressure level L_{eq} is given below where $T = t_2 - t_1$ is observation time, of A-weighted sound pressure is $P_A(t)$ and P_0 is reference sound pressure (20μPa):

$$L_{eq} = 10 \, log \left\{ \frac{1}{T} \int_{t_1}^{t_2} \frac{P_A^2}{P_0^2} \, dt \right\} \qquad (1)$$

Note: Equation adopted from [1]

3. Acoustic Noise Reduction Methods

There are different ways to approach the acoustic noise reduction, such as a vacuum enclosure of vibrationally isolated gradient assembly, a low-eddy current rf coil, and a non-conducting inner bore cryostat. Acoustic noise reduction must be done in the patient bore and in the vicinity of the magnet where physicians are positioned. In addition to that, parameter change affects the acoustic noise levels. Parameter changes can be done to the field of view, section thickness, repetition time, and echo time.

Table 1: US federal guidelines refer to the upper limits for occupational exposure to acoustic noise. No recommendations exist for non- occupational or medical exposure [2].

Permissible Exposure Levels to Acoustic Noise[a]

Noise duration/day (hr)	Sound level (dB)*
8	90
6	92
4	95
3	97
1.5	100
1	102
0.5	105
0.25	115

3.1 Gradient Noise Reduction

The gradient magnetic field is the primary source of acoustic noise associated with MR procedures. Altering the parameters varies the acoustic noise produced by the gradient field. Echo planar sequences tends to affect the acoustic noise level. Its extremely fast gradient switching times and high gradient amplitudes increase the acoustic noise levels. Decreasing slew rates decreases the noise level by 12.5 dB. Gradient noise can be reduced by minimizing echo time, as it accounts for loud signals of about 115 dB [10]. Peak noise levels are found at the low-frequency region of the spectra. An acoustic transfer function when applied to a fast spin echo (FSE) sequence measured about 0.4 dB noise level reduction [5].

Table 2: Influence of Pulse Sequence Parameters on Acoustic Noise [4]. The dBA is A-weighted decibels

Scan orientation [a]	TR ms	TE ms	FOV mm	SW mm	SPL dB(A)
Transverse	25	11	75	3	94.8 ± 2.4
Transverse	50	11	75	3	92.7 ± 3.0
Transverse	100	11	75	3	89.4 ± 3.8
Transverse	200	11	75	3	87.2 ± 4.0
Transverse	50	15	75	3	91.5 ± 1.8
Transverse	50	20	75	3	91.5 ± 2.0
Transverse	50	11	150	3	89.2 ± 1.7
Transverse	50	11	300	3	87.5 ± 0.6
Transverse	50	11	500	3	86.8 ± 0.5
Transverse	50	11	75	5	92.0 ± 3.3
Transverse	50	11	75	10	91.7 ± 3.4
Sagittal	50	11	75	3	91.1 ± 2.7
Coronal	50	11	75	3	93.6 ± 1.0

3.1.1-Parameter changes

Changes in other factors such as slice thickness, field of view and repetition time affects the acoustic noise levels. This is because there is a relationship between the TR (repetition time), FOV (field of view), and the measured noise level. The SPL increases as these parameters are reduced. Table 2 shows that reducing the FOV from 150 mm to 75 mm increases the median SPL by 3.5 dBA, reducing the TR from 50 to 25 milliseconds increases the median SPL by 2.1 dBA. There is not much influence from TE and slice width. The highest noise levels are seen with the shortest TE and smallest slice width. Reducing the slice width from 5 mm to 3 mm increases the median SPL by 0.7 dB(A), while reducing the TE from 20 to 11 milliseconds increases the median SPL by 1.2 dBA. The median SPL for the coronal plane, 93.6 dBA was greater than for the transverse or sagittal planes, with median SPLs of 91.7 dBA and 91.1 dBA. The pulse sequence parameters analysis shows that FOV and TR are more influential to noise level than field strength. Another factor that changes the acoustic noise level is the magnification. Increase in magnification increases the sound pressure level (SPL) by about 1.8 dB for every 0.5 T increase [3].

3.1.2 Acoustic Noise Distribution in the Room

Sound waves travel at the speed of 343 meters per second. As the sound waves travel away from the source of the noise, the intensity decreases as it covers more area. Similarly, the acoustic noise levels decrease as we move away from the gradient coils. Figure 1 demonstrates these phenomena. Throughout all pulse sequences, the acoustic noise around the standard scanner is the loudest as it located closest to the gradient coils.
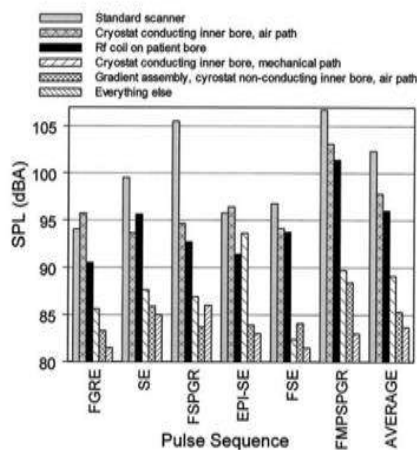

Figure 1: Bar chart showing the levels of acoustic noise applying different pulse sequences in dBA (A-weighted decibels) [4].

Figure 1 shows the different pulse sequences applied in Magnetic Resonance Imaging and the amount of acoustic noise levels recorded. The FGRE on the graph refers to fast multi echo gradient recalled echo, SE refers to Spin echo, FSPGR refers to three-dimensional fast spoiled gradient-echo, EPI-SP refers to Echo planar Imaging-Spin Echo, FMPSPGR refers to fast multiplanar spoiled gradient recalled. The bars indicate the different areas where the acoustic noise is recorded.

In addition to that, the noise measurements in the bore varies with the position along z-direction. The noise level is heard 14 cm from the isocenter near the bore entrance was about 92.7 dBA. Noise level 77 cm from the isocenter was about of 97.3 dBA. At 157 cm from the isocenter which is outside the bore, the noise level falls below 92.7 dBA [3].

This shows that the noise level varies along the z-direction with a maximum near the bore entrance [3]. Noise levels vary by 10 dB as a function of patient position along the magnet bore and an increase of from 1 to 3 dB has been measured with a patient present in the bore of the MR system which is due to the increase in pressure in the bore [5].

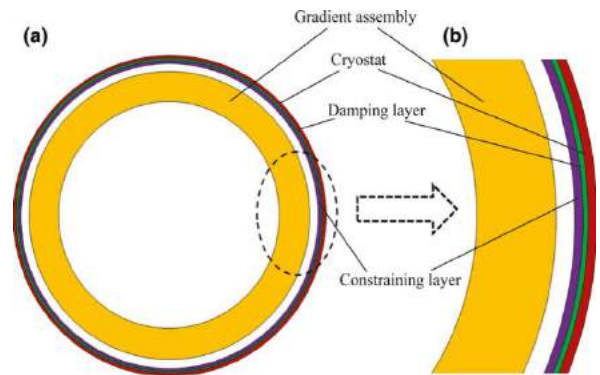### 3.2 Low Eddy Current rf Coil

Figure 2: Constrained damping treatment on the warm bore wall: an entire cross-section view (a) and an expanded view (b). [9].

Passive magnetic shims attached to the inside of the cryostat inner bore contribute to acoustic noise. They consist of 3-cm-wide strips of magnetic stainless steel glued to the cryostat inner bore. They conduct electricity. Therefore, they support eddy current driven by the gradient fields that leak out of the gradient assembly and therefore are subject to Lorentz forces that can vibrate the cryostat inner bore.

The noise contributed by metallic, conducting shims is about 88–89 dBA for the loud pulse sequences [4].

To evaluate sound pressure level (SPL) of the eddy current induced warm bore wall vibration, a Finite Element (FE) model is used. It simulates noises from both the warm bore wall vibration and the gradient coil assembly. To reduce SPL of the warm bore wall vibration, active shielding of the gradient coil must be done, which then reduced the eddy current on the warm bore wall. To control the acoustic radiation, a damping treatment can be applied to the warm bore wall. Eddy current control and damping treatment application show that the average SPL reduction of the warm bore wall can be 9.6 dB or higher in some frequency bands [9].

3.3 Dampening Bore Wall

The gradient coil was designed to leave some space for the installation of the damping materials is shown in Figure 2. The acoustic response of the warm bore wall for coil design calculated with the constrained damping layer applied results in a significant decrease in acoustic noise levels. The SPL at 1000 Hz and 1200 Hz is reduced by 6.2 dB and 23.5 dB, respectively. In the entire frequency range, the averaged SPL is reduced from 98.7 dB to 93.0 dB by the damping treatment. When both the eddy current control and damping were considered, the average SPL is reduced from 102.6 dB to 93.0 dB, a reduction of 9.6 dB. For the frequency band 100–1700 Hz that covers the majority of frequencies for gradient pulses, the averaged SPL is reduced from 105.0 dB to 88.7 dB, a 16.3 dB reduction. The overall SPL of the combined acoustic fields is reduced by 5.1 dB (from 104.2 dB to 99.1 dB) by dampening the bore wall. The presence of encased acoustic absorbent foam surrounding the magnet reduces noise levels by 3 dB (peak on A-scale) or 9 dB (RMS A-scale) [5].

3.4 Passive Noise Reduction

Acoustic noise can be reduced by mechanical ways. There are two ways to reduce the acoustic noise mechanically. One way is by reducing the noise from going out of the MRI room which can be done by using absorptive material around the MRI room, sealing wall junctions, tight-fitting doors and windows, sealing areas around penetration panels. The sound foam which uses the material polyurethane foam produces approximately 1–2 dBA noise reduction in the patient bore [4]. Sound mat which is applied to the outside of the cryostat offers 5 dBA noise level reduction in the imager room [4].

In addition to that, presence of an insulating foam mattress on the patient couch has been found to reduce vibrational coupling to the patient and noise levels by around 10 dB [6]. Ear plugs are one of the least expensive ways of noise reduction. Ear plugs, when properly used, can abate noise by 10–30 dB [5]. The passive noise reduction using ear plugs and headphones, although effective to some extent have a major disadvantage of hindering verbal communication between patients and professionals. In addition to that, one size not fit all. Therefore, many a times wearing the ear plugs are uncomfortable for patients, especially if they are worn for longer periods of time, which is standard for MRI procedures.

Another way of reducing acoustic noise is by creating a barrier around the noise source which is the gradient coils. Journal of Magnetic Resonance Imaging highlights in an article that the presence of acoustic dampers such as foam which surrounds the magnet reduces noise levels by 3 dB-9 dB [5].

3.5 Low Noise Imaging Software

Recently, there has been an increase in use of computers which has paved the way for increasing software development. The major companies producing MRI products have also developed software that decrease the acoustic noise levels. This is done by making the gradient waveforms gentle. To do this, gradient waveforms with more gradual ramp-up and ramp-down times are used. A disadvantage would be the increase in time and increase in signal to noise due to shorter windows between sampling. However, it does produce 12.5 dB decrease in acoustic noise level on average which is significant [10]. Figure 2 shows the signal with and without the noise reduction sequence optimization applied.
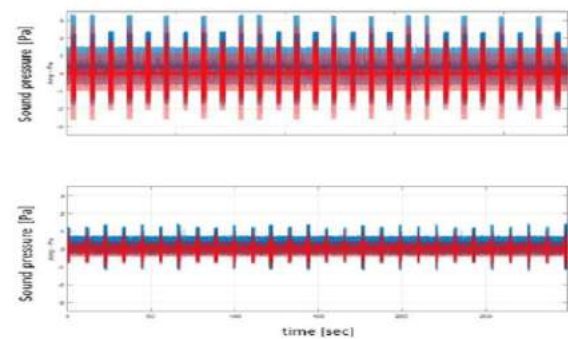

Figure 2: The top graph represents no acoustic noise reduction with peaks of 106.5 dB and the bottom graph shows the graph which acoustic noise reduction with peaks of about 97.4 dB [10]
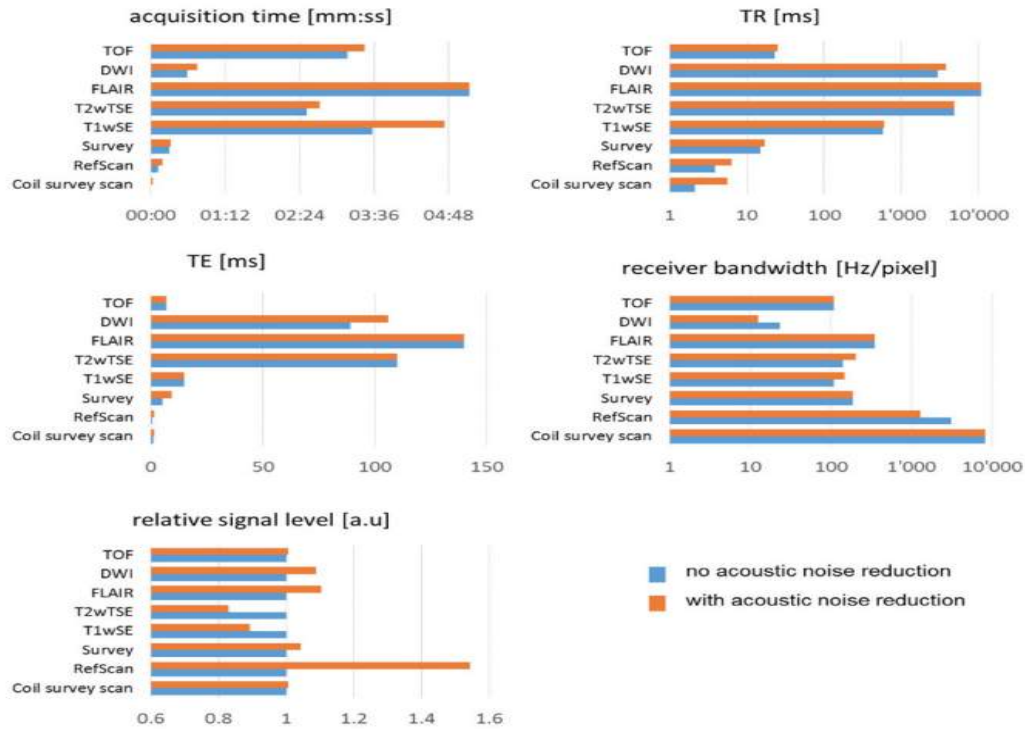
Figure 3: Overview of MR sequence parameters (acquisition time, TR, TE, receiver bandwidth, relative signal level) with and without acoustic noise reduction for six routine brain MR sequences including pre-scans (reference scan, coil survey scan) [10].

3.4.1 Side Effects Impacting Important MR Sequence Parameters

A study was conducted by Michael Wyss where two software for acoustic noise reduction were used. He used the software Softone and Comfortone to conduct his study on the effects of acoustic levels done on the parameters. These techniques reduce slew rate (rise time and fall time) of imaging gradients (slice, phase and frequency encoding). The difference between the two is that Softone allows the user to choose a reduction level between one and five while the Comfortone automatically reduces acoustic noise levels iteratively to less than 98 dB SPL [10].

Figure 3 highlights the study results with different parameters. We can observe that noise reduction technique increases the acquisition time, TR is lengthened for the coil survey scan and reference scan by about 2-3 milli seconds. The Diffusion-weighted magnetic resonance imaging (DWI) increases by about 850 milliseconds and T1 weighted Spin-Echo pulse sequence (T1w SE)

increases by about 20ms. No changes are seen for the T2 weighted Turbo Spin Echo (TSE) and the Fluid attenuated inversion recovery (FLAIR) sequence. The TE increases for the reference scan, survey scan, and coil survey scan by 1-4 milli seconds, while it increases by about 15 ms for DWI. Higher receiver bandwidth was observed for the T1 weighted SE and T2 weighted TSE and lower receiver bandwidth was observed on the reference scan and the DWI.

Using optimization techniques, an average acoustic noise control reduction of 12.5 dB was achieved. The noise reduction methods are governed by a balance between minimization of acoustic noise while keeping side effects to imaging quality minimal. Negative effects such as higher receiver bandwidth or longer TE are compensated by a longer TR. Because of this, the image quality is not compromised greatly when using acoustic noise reduction with optimization [10].

4. Discussion

The gradient noise reduction with parameters, although possible, is difficult. To significantly reduce the acoustic noise using parameters such as field of view, repetition time, slice thickness can compromise the image quality. Therefore, it is important to offset it with other parameters to make sure there is little or no compromise to image quality. The mechanical ways are the most inexpensive methods of all and therefore more popular. The software noise reduction is fairly recent, so it is not as widely used. In addition to that, the acoustic noise distribution throughout the room is different depending on the location in accordance to the noise source (gradient coil).

5. Conclusion

Most of the acoustic noise reduction methods reduce noise by about 10dB individually. To effectively reduce the acoustic noise, the different methods must be combined to give optimal acoustic noise reduction throughout the MRI room without compromising the image quality.

6. References

1. Chikai, M., Shimono, Y., Muto, K., Shibayama, H., Yagi, K., & Onodera, T. (2010). Measurement of equivalent continuous A-weighted sound pressure level of driving sound of three tesla MRI equipment. *20th International Congress on Acoustics 2010, ICA 2010 - Incorporating Proceedings of the 2010 Annual Conference of the Australian Acoustical Society* .2716-2719.

2. Cho, ZH. Park, SH. Kim JH. Analysis of acoustic noise in MRI. *Magnetic Resonance Imaging*.15:815-822,1997.

3. Price, D. Wilde J. Papadaki A. Curran J. Kitney R. Investigation of acoustic noise on 15 MRI scanners from 0.2 T to 3 T. *Magnetic Resonance Imaging*. 13:288-293, 2001.

4. Edelstein WA, Hedeen RA, Mallozzi RP, El-Hamamsy S-A, Ackermann RA, Havens TJ. Making MRI quieter. *Magnetic Resonance Imaging*. 20: 155-163, 2002.

5. McJury, M. Frank,G. Shellock. Auditory Noise Associated with MR Procedures: A Review. *Magnetic Resonance Imaging*. 12:37-45, 2000.

6. Ravicz ME, Melcher JR, Kiang NYS. Acoustic noise during functional magnetic resonance imaging. *The Journal of the Acoustic Society of America*. 108: 1683–1696, 2000.

7. Rondinoni, C. Amaro, Jr, E. Cendes, F. dos Santos, A.C. Salmon C.E.G. Effect of scanner acoustic background noise on strict resting-state fMRI. *Brazilian Journal of Medical and Biological Research.* 46(4): 359–367, 2013.

8. Ting DSW, Pasquale LR, Peng L, et al Artificial intelligence and deep learning in ophthalmology. *British Journal of Ophthalmology* .103:167-175, 2019.

9. Wang, Y. Liu, F. Zhou, X. Li, Yu. Crozier, Stuart. A numerical study of the acoustic radiation due to eddy current-cryostat interactions. *Medical Physics*.44: 2196-2206, 2017.

10. Wyss, M. Acoustic noise reduction in MRI based on pulse sequence optimization: Analysis of sound characteristics and impact on sequence parameters.*EPOS*, 2018.

IMAGE GUIDANCE SYSTEM DURING BRAIN TUMOR RESECTION SURGERY

Gabriela Wojciak
gwojci3@uic.edu

Abstract

Computer Assisted Surgery (CAS) is an umbrella term for the use of computer technology in precision planning to carry out surgical procedures; with the most famous application being Robot-Assisted Surgery. Another form of Computer Assisted Surgery is image-guided surgery which has a plethora of clinical applications in operating rooms around the world. Brain tumor resection surgery is very stressful and challenging for the surgeon because the precision and accuracy of the resection must be close to perfect to avoid hitting and cutting out any healthy tissue that may lead to neurological defects after surgery. This review article will focus on image-guided surgery in brain tumor resection. The Image Guidance System is a form of surgical navigation that revolves around the surgeon looking at preoperative CT or MRI scans conjoined with intraoperative images of the patient's anatomy during the live surgery. The surgeons then use these images to guide them during surgery via the tracking of surgical instruments. With image-guided surgery, the surgeons can locate the tumor in the brain along with the cancerous tissue surrounding it to a few millimeters aiding the surgeons with the best place to make an incision, along with giving them the optimal path they should proceed with to reach the targeted area where the tumor is located. Image guided surgery is helping minimalize invasive surgeries, shorten operating room times and giving surgeons more control over the surgical procedure.

Keywords: *Image Guidance System, Intraoperative, Brain Tumor, Image Guided Surgery*

1.Introduction

For centuries neurosurgeons have used stereotaxy to locate "targets of surgical interest within the brain relative to an external frame of reference." [3] Stereotactic surgery ('stereotaxy') revolves around attaching a metal mechanical frame to the patient's skull which would then give them information about the location of the targeted brain tumor. However accurate, it did come with its disadvantages that included discomfort for the patient leading to trauma, longer amounts of time taken to set up the system, and limited access to the patient's brain.

Figure 1. This image shows the metal mechanical frame that is mounted on the patient's head, and then through a burr hole - probe is used to reach the area of interest – the tumor.

The metal frame is used to locate the precise location of the tumor in the brain while keeping the brain from moving during surgery. [11]

Stereotaxy in neurosurgery consists of burring a small hole in the brain which gives the neurosurgeons limited access to the brain tumor intraoperatively. Thus, giving them limited space to work with if complications were to arise, such as bleeding or errors in the trajectory of the system – which is used as a guide for resection surgery. [10]

These are a few challenges neurosurgeons face during surgery; some other things they may encounter include only having preoperative imaging scans to work with and dealing with brain shift – a common side effect during neurosurgery that was once thought to be out of their control.

These disadvantages present themselves during a typical stereotactic surgery, neurosurgeons have recently turned to use image guidance during their surgeries to get live feedback of the patient's brain combined with the preoperative scans.

2. How Image Guidance System Works

During pre-op, patients get diagnostic medical imaging done such as CT or MRI. These scans allow the surgeons to devise a plan for surgery; they show the general location of the brain tumor, where the

healthy tissue is, and the critical brain structures that surround the tumor. Although surgeons know the relative location of the tumors, they are not confidently located, as diagnostic images are only relative to the state of the patient preoperatively and not intraoperatively, where unexpected/unplanned things happen all the time.

The Image Guidance System is comprised of three parts: the pre-op images, a plan surgeons devise before surgery and the live – anatomy of the patient during surgery. Image Guidance Systems are first used by neurosurgeons to devise a plan for surgery; where to make the incision, what things to avoid in the brain when resecting the brain tumor, and the path of surgery to reach the tumor with minimal damage to the patient's brain as shown in Figure 2.
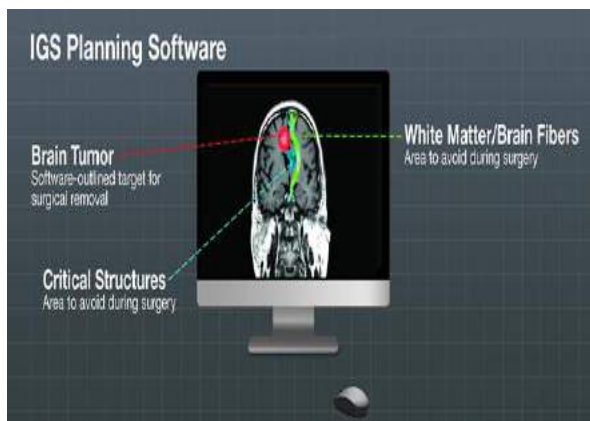

Figure 2. This image provides a visual of what a neurosurgeon sees when planning for surgery when using an image guided software. [5]

During surgery, neurosurgeons can track the medical instruments they are using via optical or electromagnetic navigation techniques. The optical technique consists of "special reflective markers on a reference instrument, which are placed close to or onto the patient's head. These reflective markers are also located on the surgical instruments and are tracked by an infrared camera, which is connected to the system's computer" [5] As the surgical instrument with the reflective marker ('pointer') is brought into the range of the infrared camera, the computer screen shows a 3D model of the brain which shows the brain tumor location and the best path that is safe to go in the brain as shown in Figure 3; which allows the surgeons to make smaller incisions in the brain.
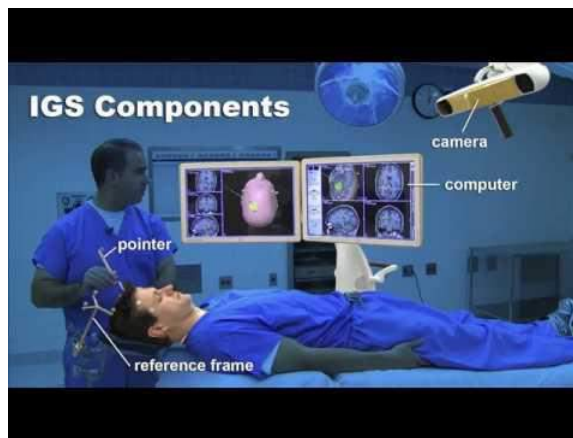

Figure 3. This image shows the components that usually make up the Image Guided System (IGS) during surgery. It consists of a computer screen, the infrared camera, a reference frame that doesn't move throughout the surgery, and the pointer which is a reflective marker that can be attached to any medical instrument. [7]

When using Image Guidance during brain resection tumor surgery, neurosurgeons must consider the expenditure of the procedure. They must justify the cost of using image guidance by proving that the patient's tumor case is proving challenging and requires this treatment. The cost of some of the image guidance systems can run up to hundreds of thousands of dollars.

3. Statistics

For several years people have argued if using Image Guidance Systems during surgeries show better results than the surgeries that do not use the system. Some studies summarized in the article Intraoperative Image Guidance in Neurosurgery state that "In a randomized controlled study, the mean amount of residual tumor tissue was 28.9% for standard surgery and 13.8% for surgery involving neuronavigation (without ioMRI)." [10] This shows that when neuronavigation (Image Guidance Systems) is being used during surgery there is a positive effect. Another study measured the median survival periods for patients who received total tumor resection for malignant astrocytoma vs. partial resection, with surgeries involving an Image Guidance System vs. ones that did not. The results of the study were 16 vs. 9 and 16 vs. 10. [10] Essentially, patients who received total brain tumor resection with surgery that used Image Guidance Systems showed to live longer than the patients who only got a partial brain tumor resection without the Image Guidance System.

Neuronavigation is a combination of imaging scans from an MRI or CT joined with extensive computer software that allows the surgeon to determine "how the direction and tip of a pointer lying out with or within the skull, relates to a two or three dimensional CT or MRI image."[9] Essentially neuronavigation is the general term used to describe any technology that is computer assisted and is used by surgeons to navigate the brain during neurosurgery. Thus, the Image Guided System falls under the neuronavigation category for surgery.

A journal from the National Center for Biotechnology Information [1] summarized several studies that were done over a long period of time, the study followed patients who had tumor resection surgery with a single space-occupying lesion. It compared neuronavigation surgery vs standard surgery that didn't use Image Guidance Systems. The results are as stated "New or worsened neurological deficits were present at three months in 45.5% of participants in the control group and 18.2% in the neuronavigation group." [1] These results show a positive effect because of using an Image Guidance System during surgery, but these next results don't show a change between the post-op patients who underwent the two surgeries.

The second result of the study states "During the first three months after surgery, seven participants (31.8%) in the control group and seven (30.4%) in the neuronavigation group experienced a new, non-neurological adverse event." [1] Such adverse events include pulmonary embolism, cardiac arrest, or cerebrospinal fluid leakage. These second results may not show a big change between the two different surgeries because after a large complex surgery like brain tumor resection, there will always be side effects after, that may or may not be controlled by the effectiveness of the surgeons' job and whether the Image Guidance System was used during surgery or not. Also, certain patients may be more prone to the amount of brain trauma they can suffer.

4. Complications: Brain Shift

"Intraoperative brain deformation, also known as brain shift, invalidates the mapping of the patient's anatomy and limits the trustworthiness of using preoperative images in intraoperative surgical navigation" [8] One big source of error that neurosurgeons encounter during brain resection tumor surgery is brain shift. Brain shift is the "movement of the brain relative to the cranium between the time of scanning and the time

of surgery."[10] This is a continuing issue that has arisen in neurosurgeries for a long time, and it is something that Image Guidance Systems need to incorporate into their system so surgeons can safely account for it if it arises during the surgery. With more specificity, intraoperative brain shifts during neurosurgical procedures are caused by "gravity, tissue manipulation, tumor size, loss of cerebrospinal fluid (CSF), and use of medication." [2] It is the most notable current limitation of any Image Guidance System. The study that investigated brain shifts during neurosurgery stated in article [2], showed that it was influenced first and foremost by the patient's head position, but it had no important effect on how big the brain shift is. The study also showed that the "angle between the main direction of shift and gravity is on average sixty degrees with a maximum of eighty-eight degrees." [2] Thus it may be possible with a few calculations to predict a general size of what the brain shift may be: according to a patient's measurements (weight, height, etc.).

There are already certain algorithms that are being researched that address the problem of brain shift by incorporating nonrigid body registration and automated intraoperative [4]. There are also several strategies/techniques that surgeons can use during the surgery to minimize the effects of the brain shift as summarized below in Table 1.

Table 1. This table summarizes certain things neurosurgeons do reduce the chances that brain shift will arise during surgery [4].

Strategies to minimize brain shift during aggressive resection of brain tumor:
- Use hyperventilation
- Avoid Diuretics, including Mannitol
- Avoid CSF diversion by spinal drain/ventricular tap/ opening of ventricles
- Mark Tumor margins before resection
- Remove tumor en bloc
- Avoid puncture of tumor cyst(s)

Hyperventilation is when someone is breathing at an abnormally rapid rate, causing decreased Pco2 levels; thus, they exhale more than they can inhale. It helps decrease the intracranial pressure allowing for safe cutting into the dura (the dura surrounds the brain and contains the cerebrospinal fluid). Once the patient undergoes this at around 20 torr, the surgeons can start resecting the tumor and once they have debulked most

of it, the intercranial pressure and hyperventilation are decreased. [4] Hyperventilation is commonly used in neurosurgeries because it puts the brain in a "relaxation" state making the brain "fuller" – thus minimizing brain shift.

As described in table 1, removing tumor en bloc helps minimize brain shifts. En bloc resections consist of the surgeon removing the whole tumor along with the healthy tissue around it [4]. This type of resection is usually preferred over piecemeal resection where the surgeons remove the tumor piece by piece avoiding the healthy tissue around it [4]. Since we are talking about neurosurgery it is critical that during the tumor resection surgery the surgeon doesn't interfere with the healthy part of the brain that may be responsible for vision, smell or hearing. When using Image Guided Systems neurosurgeons will probably be in the planning stage weighing the options of what kind of resection, they will do based on a case to case basis of the patient. If their main thing is to decrease their chances of encountering brain shift during surgery, they would opt in for the en bloc resection.

These strategies do not always work, and unexpected elements can occur during surgery; things that may end up causing a wrong cut or removal of healthy tissue - which could lead to the patients being paralyzed, losing their memory, losing their sense of smell, sight or taste. Thus, the Image Guidance System is heavily influenced by this complication because brain shift decreases the accuracy of the system intraoperatively. There are currently only a handful of new strategies that address how to accurately account for brain shift in Image Guidance Systems. Engineers are continuously investigating how to overcome this challenging complication of brain shift, and how to incorporate it in the Image Guidance System.

5. Conclusion

Although though image guided surgery has been around for nearly twenty years, it is constantly evolving. Image guidance has plenty of systems with sophisticated software that are being invented every year so the possibilities for the future are endless. The goal is to advance image-guided technology to the point where a surgeon can perform complete tumor resection with minimal possible damage to the patient's brain; so, there is no unwarranted removal of healthy tissue.

A promising aspect for the future in Image Guided Systems for surgery revolves around the system compensating for brain shift during tumor resection surgery, and the tremendous difference between preoperative and intraoperative images. A promising strategy is Feature Based Registration (FBR) which primarily registers images (the scans taken preoperatively, and the images being made during surgery with IGS) with the missing correspondences. Feature Based Registration consists of three steps "In the feature extraction step, distinctive local image features are automatically extracted and identified as key-points on preoperative and intraoperative images. In the feature matching step, a matcher searches for a corresponding intraoperative key-point for each key-point on the preoperative image. From every matched key-point pair, a displacement vector can be obtained to indicate the movement of the preoperative key-point due to the brain shift process. In the last step of FBR, the algorithm generates a dense deformation field for the entire preoperative image from the displacement vectors and uses it to map the preoperative image to the intraoperative space." [8] this strategy combined with Image Guidance Systems is in the testing phase seeing as the article introducing the method only came out in 2018. To summarize this review article image guidance systems in neurosurgery are already making an impact in operating rooms around the world but there are still things that need to be improved or invented.

6. References

1. Barone, D. G., T. A. Lawrie, and M. G. Hart. Image guided surgery for the resection of brain tumors. *Cochrane Database of Systematic Reviews*. 2014

2. Bayer, S., A. Maier, M. Ostermeier, and R. Fahrig. Intraoperative Imaging Modalities and Compensation for Brain Shift in Tumor Resection Surgery. *International Journal of Biomedical Imaging*. 2017, 2017.

3. Galloway, R. L., and R. J. Maciunas. Stereotactic neurosurgery. *Critical Reviews in Biomedical Engineering*.18:181-205, 1990.

4. Germano, I., and S. Kondo. Image-Guided Brain Tumor Resection. In: Advanced techniques in image-guided brain and spine surgery. New York: Thieme, 2002, pp. 132–140.

5. How Does Image Guided Surgery Work? at https://www.brainlab.org/get- educated/brain-tumors/understand-image-guided-surgery-for-brain-tumors/how-does-image-guided-surgery-work/. Accessed December 1, 2019.

6. Hu, S., H. Kang, Y. Baek, G. El Fakhri, A. Kuang, and H. S. Choi. Real-Time Imaging of Brain Tumor for Image-Guided Surgery, 2018. *Advanced Healthcare Materials.* 7, 2018

7. IGS, Brain Tumor Expertise at http://www.mayfieldclinic.com/brain-tumor-care.htm. Accessed December 10, 2019.

8. Luo, J., S. Frisken, I. Machado, M. Zhang, S. Pieper, P. Golland, M. Toews, P. Unadkat, A. Sedghi, H. Zhou, A. Mehrtash, C.-C. C. Frank Preiswerk, A. Golby, M. Sugiyama, and W. M. Wells. Using the variogram for vector outlier screening: application to feature-based image registration. *International Journal of Computed Assisted Radiology and Surgery*. 13:1871-1880, 2018.

9. Neurology and Neurosurgery Illustrated: Localized Neurological Disease and its Management A. Intracranial. Lindsay K., Fuller G. 2010, (fifth edition) pp. 217.

10. Schulz, C., S. Waldeck, and U. M. Mauer. Intraoperative Image Guidance in Neurosurgery: Development, Current Indications, and Future Trends. *Radiology Research and Practice*. 2012: 197364, 2012.

11. Velnar, T., and R. Bosnjak. Radiosurgical Techniques for the Treatment of brain neoplasm: A short review. *World Journal of Methodology*. 8: 51-58, 2018.

EMERGING ADVANCED OPTICAL IMAGING TECHNIQUES

Kyle Alan Luciu
kluciu2@uic.edu

Abstract

Optical imaging arguably has more uses and applications than any other imaging modality in the medical field. It has many advantages over the other imaging modalities, including cost, time, and quantity of data. One advantage that optical imaging has, it is superior resolution above other imaging modalities, this report will discuss the capabilities and technique of super resolution imaging in optics. The current uses of optical imaging, specifically in ophthalmology will be reviewed, which includes optical coherence tomography to reconstruct 3D images of a thin epidermal layer, and the derivative uses and applications that can be found in the medical field. The final section will discuss recent applications of polarization imaging sensors which provide additional information from incoming light. These sensors are biologically inspired to mimic the compound eyes found in insects. Light polarization sensor applications in the biomedical field has opened up the possibilities of research in many different aspects of bio-imaging. Current medical related experiments of light polarizing signals from biological systems will be discussed, including neural recording, dynamic tissue strength analysis, and diagnosis of flat cancerous tumors.

Keywords: *Biomedical Imaging, Optical Imaging, Super Resolution, Diffraction Limit, Structured Illumination, Phase Variance Optical Coherence Tomography (OCT), Optical Coherence Elastography (OCE), Optical Polarization Imaging, Complementary Metal-Oxide Semiconductor (CMOS) sensors, Optical Neural Recording, Degree of Linear Polarization.*

1. Introduction

Optical imaging encompasses a wide range of modalities used in biomedical applications, each serve their own purpose, and many offer advantages that commonly used medical imaging systems cannot provide. An obvious advantage is that optical imaging overcomes the danger of harmful ionizing radiation found, for example, in the case of x-ray imaging. Optical imaging is low cost, compared to the cost of production and transport of radiotracers in nuclear medicine imaging and simplistic when compared to the high amount of dynamic computations and information collected in magnetic resonance imaging (MRI) [1]. However, all medical imaging systems used are still necessary to acquire specific and vital information about the human body.

The optical imaging technique of super-resolution microscopy can provide images with resolutions exceed the diffraction limit (half the wavelength of the visible light). Many methods have been developed in order to overcome this hinderance in optical imaging systems. In certain cases, techniques have allowed the viewing of proteins and individual cell components [4]. The ability to achieve ever-increasing resolution is a clear benefactor of optical imaging systems.

A more recently developed biomedical application of optical imaging is optical coherence tomography (OCT). Light waves utilized similarly to how sound waves are used in ultrasound, can enable 3D visualization of subsurface layers in epithelial tissue [8]. OCT is very commonly found in ophthalmologists and optometrists offices for the use of studying characteristics of the internal anterior eye. OCT is particularly useful for imaging retinal and corneal tissue characteristics because of its high resolution, non-invasiveness, and cost-effective characteristics.

The most recent emergence in optical imaging discussed in this article will be optical polarization imaging. Light polarizes for a variety of reasons, therefore sensors that are sensitive to polarization can be used to detect and analyze biological phenomena that polarizes light. The polarization sensors can identify and parameterize information about a source based on light that is reflected or transmitted from the subject. In many biological systems, these polarization sensors can show us unique information that other modalities cannot. In this report, three biomedical applications for optic polarization techniques will be discussed, most of which utilize active pixel complementary metal-oxide semiconductors (CMOS) sensors [9].

2. Super Resolution Imaging

In ordinary optical imaging systems, the resolution of the system is limited to the diffraction limit of half the shortest imaging wavelength.

$$d = \frac{\lambda}{2NA} \qquad (1)$$

While NA is the numerical aperture of the lens used. The discussed method of overcoming the diffraction limit will be due to the wavelength properties of light. In terms of the spatial frequency and light and dark field illumination.

2.1 Diffraction Limit

Higher resolutions can be achieved through multiplexing reference and sample spatial frequency bands [3]. This essentially means superimposing a subject wave pattern with a secondary reference imaging light. The secondary light must have a set frequency, that has a constructive property relative to the reference wavelength light fringes. The constructive property at the reference light fringes, once superimposed results with an image that has more complex frequency components, which can be deconstructed to form an enhanced resolution image. The final image can be backwards Fourier transformed and filtered to eliminate the higher frequency "distortion signal" and leave the high-resolution image. This allows sub-wavelength resolution, which is normally the diffraction limit of about 0.2 μm [4].
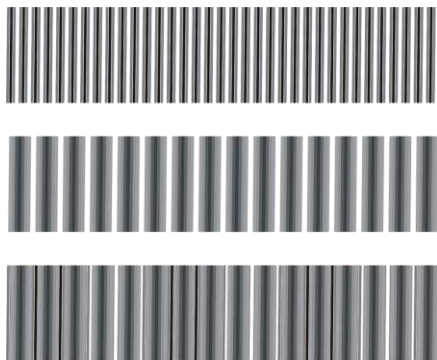

Figure 1: The structured illumination technique of super-resolution. Top row: Targeted resolution band. Second row: Secondary light. Third row: Superimposed spatial frequencies [3].

The first row is the diffraction limit of the reference light depicted in spatial frequency with the dark grey depicting the diffraction limit fringes. The second row, the chosen secondary frequency pattern is incidentally superimposed on reference light on the subject surface. The third row shows the overlaying of the first and second row, and that the fringe components can be formed within the diffraction limit, and therefore providing an enhanced version of the original image.
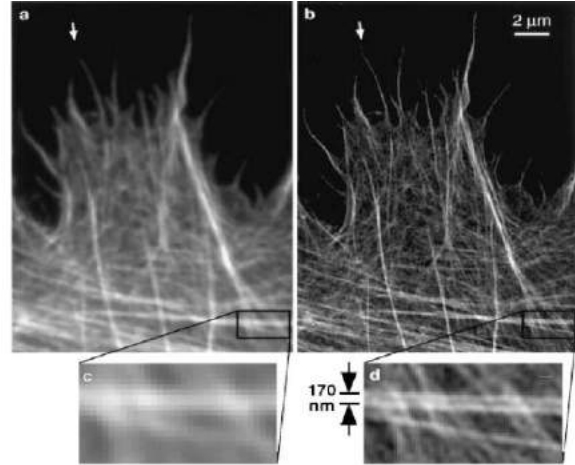

Figure 2: Actin cytoskeleton at the edge of a HeLa cell. (a) 280-300 nm resolution, (b) 110-120 nm resolution, (c) enlarged conventional microscopy image, (d) enlarged structured illumination technique applied image [4].

3. Phase Variance Optical Coherence Tomography

3.1 Phase Variance OCT

Phase variance OCT allows for volumetric imaging of retinal or general microvasculature networks. This makes it different from the OCT machines that you might find in an Optometrist's office which often display slices or 2D images. Phase variance OCT is the replacement for intravenous fluorophore injections for measuring volume in retinal vasculature. It is beneficial for diagnosing diseases and monitoring the age-related macular degeneration or the effects of medicine or recovery of eye surgery patients over time. In order to obtain a phase variance OCT, the phase change and phase variance must be calculated. Phases will be varied at the same location of a scan in order to generate a 3D image of the microvasculature structure.
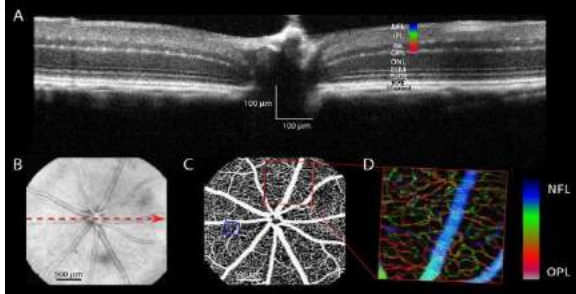
Figure 3: Phase variance OCT allows for 3D imaging of the optic nerve and major blood vessels. (a) Cross sectional image of OCT scan in grey scale. (b) Projection of vessel width by OCT rendering, (c) Phase variance boundary condition analysis of the OCT projection, (d) Vessel depth is color coded based on phase variance scale in (a,d) [6].

3.2 Differential Artery and Vein Analysis

OCT Angiography allows for the 3D visualization of retinal vascularization. The processing of the 3D images allows diagnosis, monitoring, and detection of signifying changes seen in the vascularization characteristics of a patient. The many quantitative features that OCTA can classify are: Blood vessel tortuosity, blood vessel caliber, blood vessel density, vessel perimeter index, foveal avascular zone (FAZ) area, FAZ contour irregularity, and branch-point geometry. These analytical measurements can help medical professionals determine the diagnosis of a retinal disease. All of these analysis techniques are conducted using analytical and imaging software such as MATLAB [8].

3.3 Optical Coherence Elastography

Much like the use of ultrasound imaging, elastography techniques can be applied to OCT to form optical coherence elastography (OCE), which is used to detect depth-resolved sample deformation in OCT images. The sample structures being imaged are observed for displacement under Young's modulus. OCE can be used to detect abnormalities in or beneath surface tissues such as tumors.
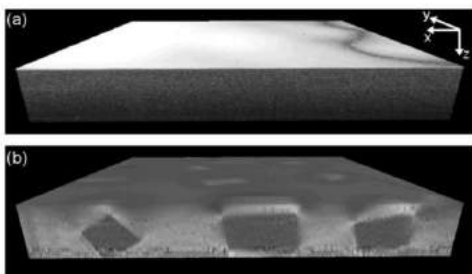

Figure 4: (a) OCT image reconstruction highlights optical contrast. (b) OCE image of a phantom highlighting the mechanical contrast in a phantom [8].

OCE probes can even be injected near tumor sites guided by ultrasound to gather physiological details of the target sample.
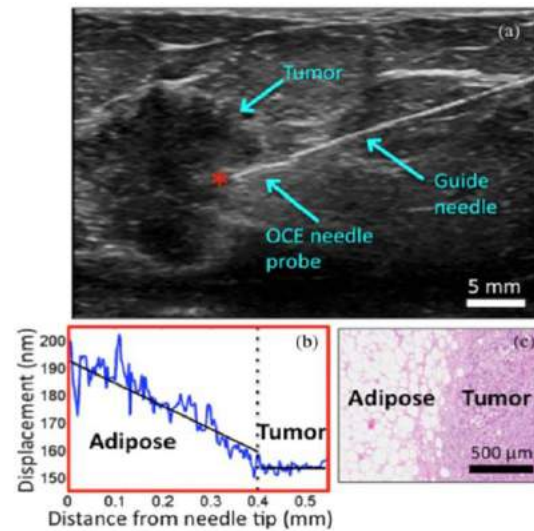

Figure 5: OCE probe case study used to determine characteristics of irregularities in specimen. (a) Ultrasound tumor case study image of OCE probe, (b) Ultrasound signal contrast, (c) Resulting OCE image of fat-tumor interface [8]

4. Optical Polarization Imaging

The basis of optical polarization imaging is detection of the amplitude and rotation of polarized light. The detected light is either reflected or transmitted through the subject of interest or reflected off of the subject. The result is a wave of incident light that is polarized some way during the process. The output light can be analyzed for the subject's polarization properties mathematically. The Stokes parameters describe these variables of amplitude and orientation of light as an electric field, since it is fundamentally an electro-magnetic wave. The behavior of polarization is either linear, circular, or components of both polarizations.

4.1 System and Components

Noninvasive techniques using light source, and detectors take advantage of optical polarization in biomedical applications. Complementary metal-oxide semiconductors (CMOS) sensors are active pixel optical sensors organized in an array which can be used to determine the polarization of a wide field of light. CMOS scanners therefore are able to analyze and differentiate a light source containing common, or complex polarization components.
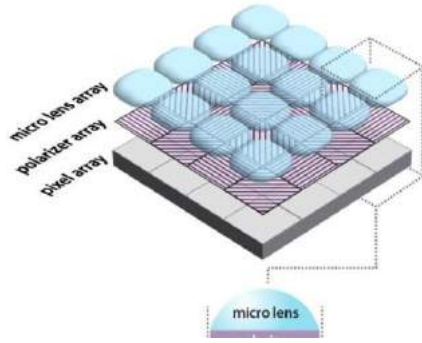
26

Figure 6: CMOS Diagram: Convex lens array converges light onto polarization filters and assigns intensity by pixel-semiconductors [9].

CMOS sensors are widely used for analyzing the light polarization properties of surface characteristics and identifying material composition, therefore are beneficial in the biomedical field. Experiments focus on discover if direct correlations between biological phenomena of interest and light polarization can be found [7]. Three emerging biomedical applications of optical polarization imaging will be discussed in this report.

4.2 Optical Neural Recording

Optical neural recording has pushed forward development in the neuroscience field by increasing observational field of view of neural activity. In this experiment, a biologically safe wavelength of 625 nm LED lights (orange/red). When, incident, unpolarized light is reflected off of the nerve tissue, a reflecting linearized polarized light propagates back. The neuro-electrical signal observed is from a locust's olfactory neuron with electrical probes. The polarization of the reflected light from the locust neural activity is characterized by the observed change in the reflected polarization angles [9].
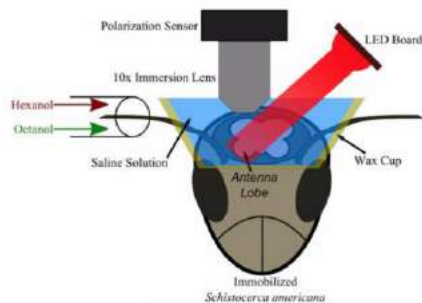

Figure 7: Experimental apparatus for electrical characterization, in recording locust olfactory neuron activity experiment [3].

The locust olfactory nerve is submerged in a saline solution which also serves as an immersion median for the 10X lens. Two odors, hexanol and octanol are introduced to the antennae, in order to achieve the stimulation of an action potential across the target olfactory neuron. The polarization response is recorded by a CMOS sensor. The activity is proportional to the change in voltage across the olfactory neuron during the experimental activation periods. This information introduces a new opportunity of advancement in observing large areas of neural activity which is vital information when studying neurobiology. This is only an example of the olfactory response, but the same imaging techniques, under different experimental settings, can be used to quantify responses in other neural fibers as well [9].

4.3 Soft Tissue Stress Analysis

Bio-inspired polarization optics can also be used to make mechanical measurements as well. In this experiment, collagen fibers undergoing varying accelerations of strain are examined in order to better understand the structure-function of loading conditions. Traditional measurements take a longer time than real life conditions because they involve fixed strain on the collagen fibers followed by a rotation of the sample to record a full view. In this experiment, a thin strand ($300 \ \mu m$) of a bovine tendon is used to observe the tissue's mechanical response under different loads and orientations. The tendon is held by clamps attached to a computer-controlled actuator which applies cyclical strain at 1 Hz.
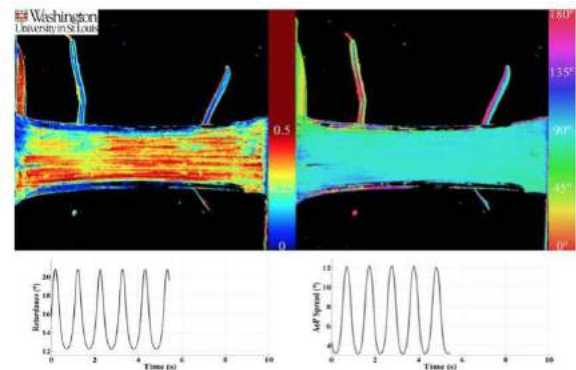

Figure 8: Cow tendon under load. (Left) degree of linear polarization heat map. (Right) Angle of polarization heat map [9].

The transmittance of light through the loaded tissue shows how the tendon displays different polarization responses based on different strain demands, the two measurements polarization measurements taken are the degree of linear polarization, and the angle of

polarization. They are functions of the Stoke's parameters of the experimental conditions. Where the linear polarization shows fiber parallel uniformity, and the angle of polarization shows the angle of the fiber. When the tendon is subject to maximal strain, a high linear polarization response is observed. This work shows how polarization imaging can be extremely useful for soft tissue stress analysis in dynamic tissue loading. With more experimental possibilities, this modality has proven to contribute to a better understanding of sports related injuries in the medical field and can assist in developing in vivo monitoring implants or prosthetics with higher biomechanical fidelity [9].

4.4 Imaging Flat Cancerous Tumors

Polarization imagers with CMOS sensors can be attached to the tips of endoscopes to improve the detection of flat lesion malignant tumors. Currently, regular endoscopes are used to identify flat lesion tumors. However, the majority (50-80%) of these tumors go undetected due to the visually hard to distinguish, nature of the tumors in comparison to healthy GI tract tissue. It has been proven that flat lesion tumors display lower levels of DoLP due to the abnormal composition and fiber orientation of the tissue. With the use of infrared fluorescent dyes along with CMOS scanners, these experiments have proved that flat lesion tumors are more recognizable under polarization imaging conditions. The figure below shows the experimental result found by this method.
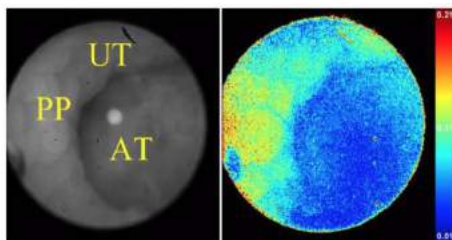

Figure 9: Endoscopy images (Left) regular and (Right) fluorescence polarization endoscope with DoLP correlation heat mapping. UT: Uninvolved tissue, PP: Peyer's patch, AT: Adenomatous tumor [9].

the DoLP signal is a more capable detection method for identifying flat tumors. DoLP analysis ranges from 0 to 0.21 in the image above, and uses the parameters of 0.0414 for tumors, 0.0225 for flat lesion tumors, and 0.0816 for unaffected tissue to determine affected areas. Parameters can be adjusted further with machine learning to tailor cutoffs to individual patients. The use of CMOS sensors on the tips of endoscopic cameras is highly feasible for detecting cancerous tumors and can only be made more effective

with the development of nanofabrication technologies and methods [9].

5. Conclusion

The benefactors of optical imaging have already proved to be exceptional. With their lower cost, faster speeds, unmatched resolution, and versatility, optical imaging systems and their emerging sub-modalities are sure to warrant increasing attention and development in the future. The potential for optical imaging to develop quickly is amplified by its applicability in many fields besides medicine. Satellites primarily use optical systems as well as cell phone and laptop imaging systems.

The applications of super resolution methods in the study of cell behavior and structure show great promise in better understanding the world on the nanoscale. The uses of OCT and OCE to create volumetric images of soft tissues using only optical measurements, contradicts to the belief that optical imaging can only produce two dimensional images. Rather, these methods open a whole aspect of non-invasive imaging that use light waves in near-real time, similar to sound waves in ultrasound.

Optical polarization imaging is the most recently developed mentioned system in this article. It is particularly interesting because of its wide variety of uses. Although these systems are not being commercially produced and used for the medical field, they are unique capabilities will likely find them a spot in clinical imaging in the near future.

6. References

1. Amoozegar, C. B., E. M. Hillman, C. B., T. Wang, F. H. McCaslin, M. B. Bouchard, J. Mansfield, R. M. Levenson. In vivo optical imaging and dynamic contrast methods for biomedical research. The Royal Society Publishing. 2011.

2. Debajit S, K. Leong, N. Katta, B. Raman. Multi-unit recording methods to characterize neural activity in the locust (Schistocerca Americana) Olfactory Circuits. *Journal of Visualized Experiments.* 71, 2013.

3. Farsiu S., D. Robinson, M. Elad, P. Milanfar. Fast and Robust Multiframe Super Resolution. *IEEE Transactions on Image Processing.* 13: 1327, 2004.

4. Gustaffsson, M. G. L. Surpassing the lateral resolution limit by a factor of two using structured illumination microscopy. *Journal of Microscopy*. 198: 82–87, 2000.

5. Larin, K. V., D. D. Sampson. Optical coherence elastography – OCT at work in tissue biomechanics. *Biomedical Optics Express.* 8:1172-1202, 2017.

6. Mohammed S. M, D. W. Cadotte, B. Vuong, C. Sun, T. W. H. Luk, A. Mariampillai, V. X. D. Yang. Review of speckle and phase variance optical coherence tomography to visualize microvascular networks. *Journal of Biomedical Optics* .18, 2013.

7. Sarkar, M., A. Theuwissen. A Biologically Inspired CMOS Image Sensor. Springer-Verlag Berlin Heidelberg. SCI 461, pp. 105–155, 2013.

8. Yao, X., T. H. Kim, T. Son, Y. Lu, M. Alam. Comparative Optical Coherence Tomography Angiography of Wild-Type and rd10 Mouse Retinas. *Translational vison science and technology*. 7:42, 2018.

9. York, T., et al. Bioinspired Polarization Imaging Sensors. *Proceedings of IEEE*. 102: 1450-1469, 2014.

MONITORING DIABETIC NEPHROPATHY DISEASE USING INFRARED SPECTROSCOPY

Osayd Nazzal
Onazza2@uic.edu

Abstract
Histology is the current gold standard of collecting biochemical information (protein, lipids, DNA). However, routine histology involves staining or dyeing biomolecules after biopsies. Stained biopsies may be a practical limitation due to inconsistency in staining. Although, such quantitative techniques have advanced, the time required for obtaining multiple stains is still a limitation factor. An emerging modality, Fourier Transform Infrared (FT-IR) Spectroscopy is a new approach for label-free molecular analysis and chemical imaging. The base principle of FT-IR imaging is that different regions of the mid-infrared are absorbed through different chemical bonds within the tissue (or cell), which can be related to the presence and composition of biomolecules. Furthermore, Infrared (IR) imaging uses computational methods that do not require human supervision, as opposed to staining. Nevertheless, there is an unfulfilled clinical need to allow for earlier diagnosis and risk stratification. IR imaging is a non-invasive, cost effective approach that can be used to detect renal related diseases (diabetes in this case) with high accuracy. In this paper, we demonstrate Infrared Spectroscopy technology that has been employed to better predict the development of diabetic nephropathy.

Keywords: *Infrared, Spectroscopy, Kidney disease, label-free imaging.*

1. Introduction

Approximately, 20-40% of diabetic patients develop diabetic nephropathy, a long-term chronic kidney disease and the primary cause of end-stage renal disease (ESRD) [4,6]. Kidney transplantation is often an effective treatment for ESRD [4]. However, approximately 25% of 1-year post-transplants recipients experience chronic allograft injury ultimately leading to allograft failure [5]. A widely accepted method to monitor allograft for complications post-transplantation is serum creatinine (SCr) [4]. However, several non-renal factors such as age, gender, and body mass can influence creatinine [16]. Unfortunately, complications are detected after a decline in the renal function [3,4]. Despite the improvement of the immunosuppressive strategies, chronic allograft injury remains the primary cause of renal allograft failure. These complications are defined as a slow decline in renal function, high blood pressure, and proteinuria and are often not seen until 2 years after transplantation [4]. Therefore, there is a lack of advanced tools to predict the graft outcome and an unmet clinical need for early detection of complications. Also, the liver is one of the organs that could be affected by diabetes. As an organ with various functions that are essential for our body's metabolism, the liver is also at risk of chronic diseases. Liver fibrosis is caused by various reasons one of which being alcoholic hepatitis [6,12]. Although the liver demonstrates a remarkable ability to regenerate tissue, repeated cycles of damage can quickly lead to inflammation and fibrosis [16]. Furthermore, liver biopsies from diabetic patients may show distinct chemical changes, therefore, understanding the differences in regions of fibrosis is essential to obtain diagnostic information [12].

Recent dramatic advances have transformed IR imaging from a research tool into a potentially powerful clinical tool, providing insight in a label-free, cost effective, and non-perturbing manner into the biochemistry of tissue [7,13]. IR imaging represents a useful adjunct to current pathology techniques due to its ability to provide complementary biochemical information that would otherwise not be accessible using conventional staining approaches [17]. The spectral data obtained from FTIR spectroscopy provides rapid quantitative and qualitative measurements of biochemical

changes. Previous work has demonstrated that damage and disease in an organ such as the kidney leads to changes in the IR absorption spectra of the tissue [8]. Moreover, recent studies have shown that different structures in the kidney are chemically modified due to diseases such as diabetes and these changes can be detected before morphological changes become apparent [2,14]. As a result, FTIR spectroscopy is becoming increasingly applied as a potential diagnostic tool for kidney diseases [16]. FTIR surpasses many digital imaging techniques in that FTIR is capable of quantifying fibrosis and inflammation at the same time. Current techniques that are based on digital imaging analysis such as Masson Trichrome and Red Sirius present limitations. Since both techniques are based on collagen staining, an important limitation is confusion of constitutive and pathologic collagen, also we can only quantify fibrosis or inflammation not both at the same time [5].

1. Theory

In spectroscopy, it is important to know which frequencies absorbed for individual frequencies of radiation need to be analyzed. For this reason, the radiation source must cover a broad spectral range [6]. A common spectrometer consists of a source, interferometer, sample compartment, detector, amplifier, A/D convertor, and a computer [1]. In a conventional spectrometer often known as "Dispersive spectrometer" a prism is used to disperse light into the individual frequencies and then a slit, determining which frequency will reach the detector, is placed in front of the detector. On the contrary, an FTIR spectrometer obeys the principle of Fourier transform, which can be expressed mathematically as shown in equation (1).

$$F(\omega) = \int_{-\infty}^{+\infty} f(x)e^{i\omega x}dx \qquad (1)$$

where ⍵ is the angular frequency, x is optical path, f (x) is the interferogram, F(⍵) is the spectrum, and i equal to the square root of minus one. The interferogram is determined experimentally in an FTIR spectroscopy, also the corresponding spectrum frequency is determined using Fourier transform which then is plotted against intensity [3]. The interferometer in an FTIR spectrometer is usually Michelson type (Fig. 1) and is replacing the monochromator. Furthermore, the interferometer consists of one stationary mirror and one adjustable mirror dividing beams into two through the means of a beam splitter: [1]. The beam splitter is designed such that it only transmits and reflects half of the light [3].
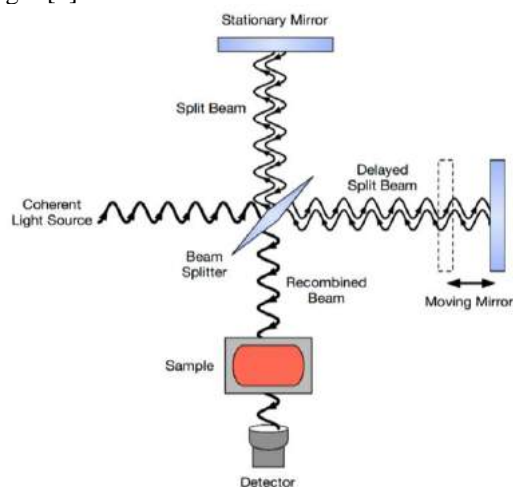

Figure 1. Schematic of Michelson interferogram. Adapted from Birkner [3].

An infrared spectrum represents a fingerprint of a sample with absorption peaks corresponding to frequencies of vibrations between atoms. Since each material has unique combination of atoms, no two compounds produce the exact same spectrum. As a result, IR imaging can result in a positive identification of every different material. Moreover, the size of the peak in the spectrum is an indication of the amount of material present.
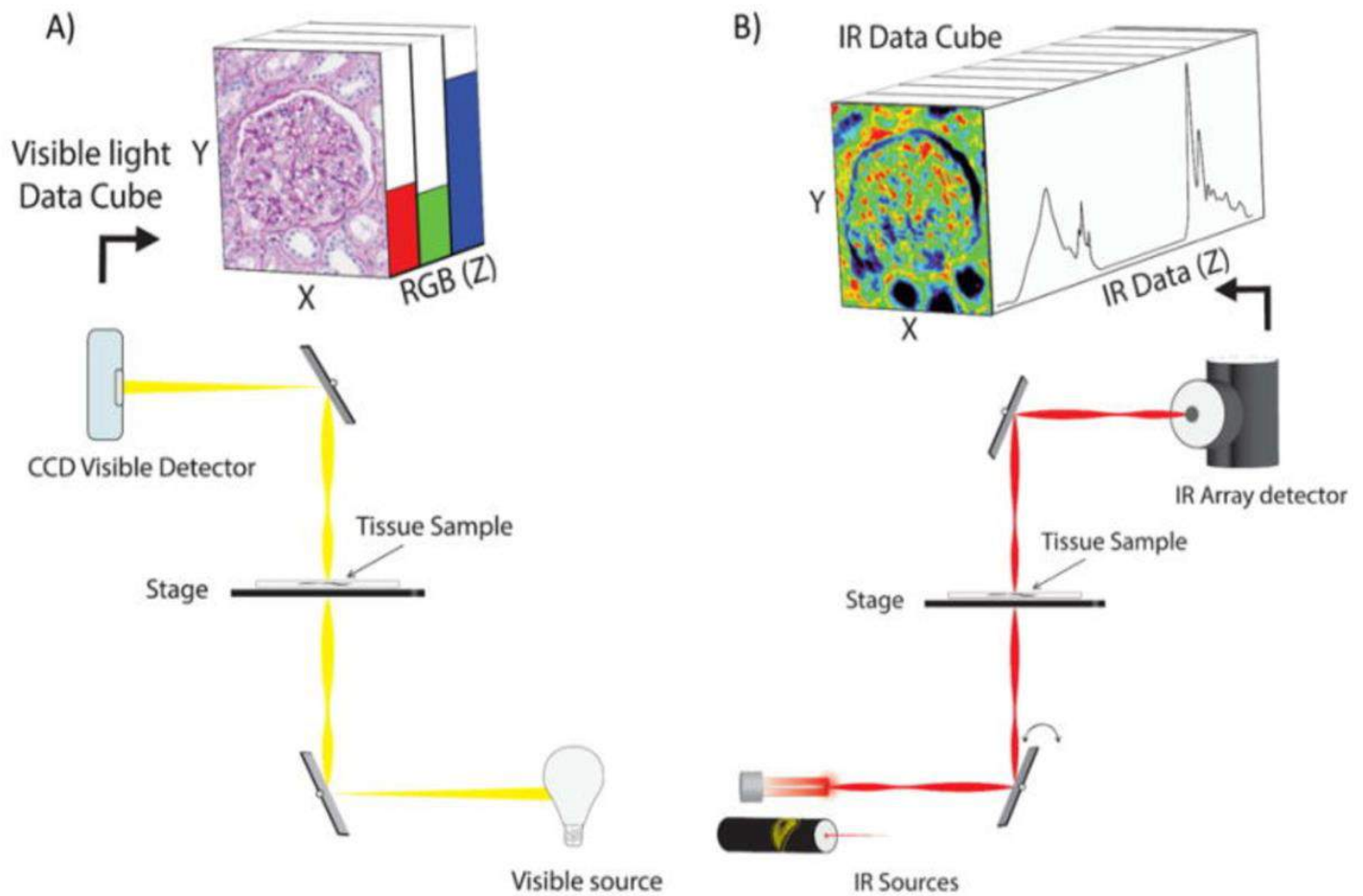
Figure 2. Schematic of a typical IR system [1]

3. Methods

IR imaging is subject to FTIR protocols. In a manuscript [2] written by leaders in the field, the standard methods and procedures are described in detail. Figure 2 is an illustration of an FTIR set-up in a lab. An IR system has both visible and IR light source/detection system (Figure 2.A). The visible light source is used to visualize the sample and find the region of interest on the tissue section [2,4,13]. The charge coupled device (CCD) visible detector in the system collects the visible light and creates a data cube with an RGB image coupled with spatial dimension. After the region is found, the mirrors in the system flip to the IR source/detector, and an IR source is used to obtain an image. As mid-IR passes through the sample, different regions are absorbed by different biomolecules to give a biochemical fingerprint of the tissue, which is collected using a detector sensitive to IR,

creating an image (Figure 2.B) [2,4,14]. Three vital steps that were followed prior to scanning any FTIR sample. First, we prepared the tissue sample. One section of a formalin fixed paraffin embedded tissue block was placed on Barium fluoride (BaF_2) slide. Moreover, tissues that were used for IR analysis were deparaffinized. Second, we prepared the slide by cooling the FTIR detector to 79K using liquid nitrogen. Depending on the size of the sample that was being scanned, it is very important to keep the detector cold, therefore we poured liquid nitrogen every six hours. Last, before collecting data from the sample, we collected a background spectrum first, to ensure we could subtract any unwanted residual peaks from our sample spectrum after scanning [2].

4. Results

In a study conducted by Varma et. al [14], five transplant patients had ESRD caused by diabetes. The patients had stable allograft function, undergone protocol post-transplant biopsies, 3-6 months post-transplant (early transplant), and post-transplant (late transplant). Typically, these biopsies of post-transplant patients are checked for any complication post-transplantation. The study found three of five patients had diabetic nephropathy related histological changes and the early (3-6 month) biopsies had no clinical or histologic evidence of diabetic nephropathy. Recurrent and non-recurrent diabetic nephropathy in late biopsies was associated with distinct clusters in the early biopsies. This phenomenon suggests that underlying biochemical changes occur even in the absence of histologic evidence of diabetic nephropathy. Thus, IR imaging may allow for the detection of diabetic nephropathy in transplanted kidneys earlier than is morphologically evident. In another study developed by Brunye et. al [4], the result obtained by Varma et. al [13] aligned with the results found in their experiment [4], it is worth noting that the study conducted by Brunye had more patients, 65 patients to be exact.

A study was conducted Sreedhar et al. [12] at the University of Illinois at Chicago (UIC). The author demonstrated that IR spectroscopic imaging easily discriminated between hepatocytes and fibrosis regions as shown in figure 3, which was achieved using a

classifier: Principle Component Analysis accompanied with Linear Discriminant Analysis (PCA-LDA) [12]. They found that regions of hepatocytes for diabetic patients displayed high degrees of intra-class variance. The source of variance is believed to be the accumulation of glycogen in the liver and contribution of clear cell inclusions of liver disease according to Sreedhar [12]. Glucose, fat, and water are typically found in clear inclusion as part of the liver disease [8]. In this study, IR images were acquired from 20 patients; 10 patients were diagnosed with diabetes, while the other 10 were healthy. The purpose of this study was to explore the impact of diabetes on the liver. The results unveiled that the regions of fibrosis are clearly separated.

5. Conclusion

Results have demonstrated that IR imaging spectroscopy has a greater potential for becoming a diagnostic tool soon to predict outcomes of diseases such as kidney nephropathy and liver fibrosis. The ability to detect complications before the organ functionality is reduced is critical. Often, these complications are not detected until 2 years later using conventional methods such as histology for patients' post-transplantation. In addition, studies have shown
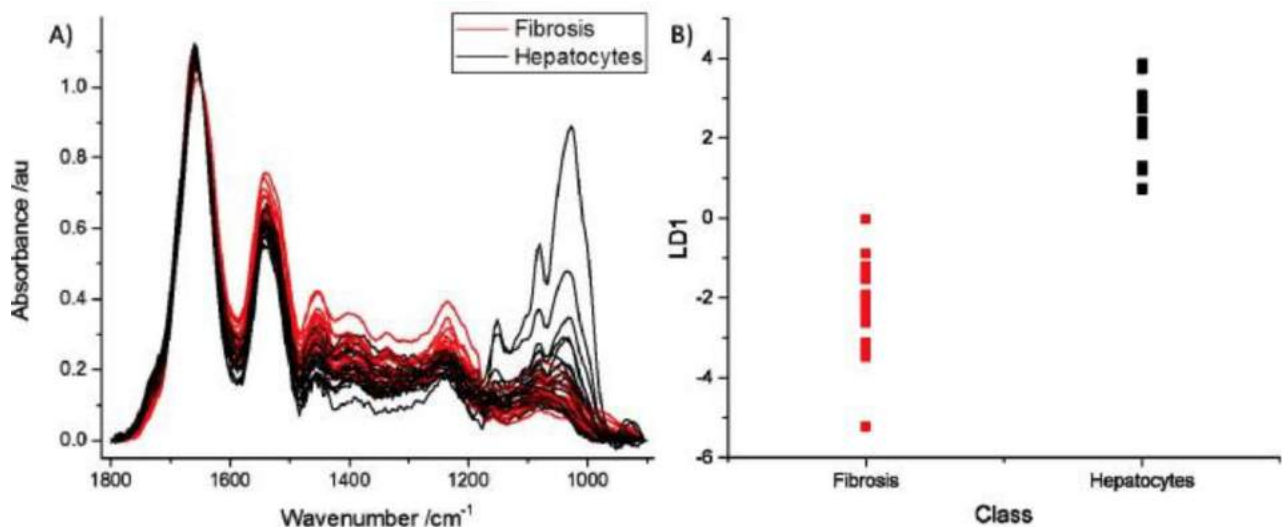

Figure 3. A) illustrates the average spectra from regions of fibrosis and hepatocytes for diabetic and non-diabetic patients. B) Using PCA-LDA, both regions of fibrosis and hepatocytes are distinguished.
This figure is adopted from Sreedhar [12].

33

that in organs, such as the liver, hepatocytes may indicate chemical changes and understanding these changes is essential for diagnosis. The results of the conducted experiments form the foundation of future studies to better predict patient outcome, diagnosis, and identify high risk patients. Current advancement of FTIR made it possible to obtain data that otherwise may not be accessible. QCL approaches have greater advantages among conventional FTIR for their improved speed that allows for rapid collection of wavenumbers in regions of interest. To conclude, IR imaging with its sensitivity to biochemical differences in regions of fibrosis and capacity for high-throughput in assessing tissue sample is very well positioned to be an investigative tool in liver histopathology and kidney nephropathy that are often-overlooked.

5. Discussion

IR imaging allows for the acquisition of images wherein each pixel is a mid-infrared spectrum. Therefore, the IR tissue image will display contrast based on the absorbance of biochemistry [6]. A new advancement in mid-IR imaging has come in the form of tunable mid-infrared quantum cascade lasers (QCL) that allow for high-intensity discrete-frequency measurements and live imaging by exploiting the full laser brightness at selected wavelength which is potentially advantageous in deployment of IR imaging in the pathology clinical setting [7,9]. Furthermore, using QCL approaches, researchers can highlight regions of interest: single discrete frequency [5]. That is, to allow for rapid collection of wavenumbers in region of interest across a tissue sample. Treatment for diabetic nephropathy is often not very satisfying because renal involvement is discovered too late using the conventional diagnostic techniques [5].

As demonstrated in the results, fibrosis to a lesser degree can be altered biochemically by the status diabetes of patients and that it can be detectable using IR spectroscopy. But future studies can explore whether the level of diabetic damage to liver tissue can be observed using only a few discrete spectral frequencies. This would create an advantage for QCL based discrete frequency imaging approaches where they can leverage a greater speed than conventional FTIR approaches. Since biochemical alterations precede histopathological changes, early IR imaging identification of diabetic nephropathy could be useful to complement histopathological analysis to prevent or delay further disease progression with more focused interventions, especially in the setting of post kidney transplantation biopsies. In addition, IR spectroscopy may also be helpful in monitoring the effect of instituted therapies [4]. Future research could focus on the potential of the spectral features as prognostic biomarkers for progressive diabetic nephropathy.

Nevertheless, studies on a larger number of patients are needed to confirm the external validity of the results. Full validation studies with adequate training and test sets must be designed.

6. References

1. <https://www.spectralpathology.com>. Accessed June 5, 2019.

2. Åmand, Lars-Erik. "The Theory Behind FTIR Analysis." The Centre of Combustion Science and Technology, *Semantic Scholar*, 1999.

3. Baker MJ, Trevisan J, Bassan P, et al. Using Fourier transform IR spectroscopy to analyze biological materials. Nature proto-cols. 9:1771–1791, 2014.

4. How an FTIR Spectrometer Operates. <chem.libretexts.org/Bookshelves/Physical_and_Theoretical_Chemistry_Textbook_Maps/Supplemental_Modules_(Physical_and_Theoretical_Chemistry)/Spectroscopy/Vibrational_Spectroscopy/Infrared_Spectroscopy/How_an_FTIR_Spectrometer_Operates>. Accessed June 5, 2019.

5. Bruyne, Sander De, et al. Detection and Characterization of a Biochemical Signature Associated with Diabetic Nephropathy Using Near-Infrared Spectroscopy on Tissue Sections. *Journal of Clinical Medicine*. 8: 1022, 2019.

6. Grimm PC, Nickerson P, Gough J, McKenna R, Stern E, Jeffery J, Rush DN. Computerized image analysis of Sirius Red-stained renal allograft biopsies as a surrogate marker to predict long-term allograft function. *Journal of the American Society of Nephrology*. 14: 1662–1668, 2003.

7. J. C. Hsiang, E. J. Gane, W. W. Bai, and S. J. Gerred. Type 2 diabetes: a risk factor for liver mortality and complications in hepatitis B cirrhosis patients. *Journal of Gastroenterology and Hepatology*. 30: 591–599, 2015.

8. K. Yeh, S. Kenkel, J. N. Liu, and R. Bhargava, Fast infrared chemical imaging with a quantum cascade laser. *Analytical Chemistry*. 87:485–493, 2015.

9. Martak, Daniel, et al. Fourier-Transform InfraRed Spectroscopy Can Quickly Type Gram-Negative Bacilli Responsible for Hospital Outbreaks. *Frontiers in Microbiology*. 10:1440, 2019.

10. M. Diem, L. Chiriboga, and H. Yee. Infrared spectroscopy of human cells and tissue. VIII. Strategies for analysis of infrared tissue mapping data and applications to liver tissue. *Biopolymers*. 57: 282–290, 2000.

11. M. Walsh, M. Barre, B. Bird, H. Sreedhar, V. Varma, A. Graham, Z. Richards, F. Gambacorta, A. Bhatt, P. Nguyen, K. Meinke, L. Nonn, G. Guzman, E. Fotheringham, M. Weida, D. Arnone, B. Mohar, and J. Rowlette. Using QCLs for MIR-based spectral imaging – applications in tissue pathology. *Biophotonics*. 2015.

12. P. Wang, D. Kang, W. Cao, Y. Wang, and Z. Liu, Diabetes mellitus and risk of hepatocellular carcinoma: a systematic review and meta-analysis. *Diabetes/Metabolism Research and Reviews*. 28:109–122, 2012.

13. Sreedhar, Hari, et al. Infrared Spectroscopic Imaging Detects Chemical Modifications in Liver Fibrosis Due to Diabetes and Disease. *Biomedical Optics Express*.7: 2419, 2016.

14. Varma, Vishal K., et al. A Label-s Free Approach by Infrared Spectroscopic Imaging for Interrogating the Biochemistry of Diabetic Nephropathy Progression. *Kidney International*. 89: 1153–1159, 2016.

15. Varma, V. K., Kajdacsy-Balla, A., Akkina, S., Setty, S., & Walsh, M. J. Predicting Fibrosis Progression in Renal Transplant Recipients Using Laser-Based Infrared Spectroscopic Imaging. *Scientific Reports*. 8 :686, 2018.

16. V. K. Varma, S. Ohlander, P. Nguyen, C. Vendryes, S. Parthiban, B. Hamilton, M. C. Wallis, A. Kajdacsy-Balla, B. Hannaford, T. Lendvay, J. M. Hoatling, and M. J. Walsh .Fourier transform infrared spectroscopic imaging identifies early biochemical markers of tissue damage. *Proceedings SPIE* .8939, 2014.

17. Vuiblet, Vincent, et al. Renal Graft Fibrosis and Inflammation Quantification by an Automated Fourier–Transform Infrared Imaging Technique. *Journal of the American Society of Nephrology*. 27:2382–2391, 2015.

18. Walsh, M. J., et al. Label-Free Biomedical Imaging With Mid-IR Spectroscopy. *IEEE Journal of Selected Topics in Quantum Electronics*. 18: 1502–1513, 2012.

REVIEW OF CLINICAL PHOTOACOUSTIC IMAGING

Ricardo Rodriguez

rrodri79@uic.edu

Abstract

Photoacoustic imaging (PAI) is a new, hybrid, non-ionizing, and non-invasive imaging technology that makes use of sound waves to create high-resolution images. Its potential for a wide range of medical applications has led researchers to propose its integration into the clinical setting. However, PAI's limiting factors of penetration depth, equipment fabrication, cost, and lack of FDA approved contrast agents have kept PAI from bedside availability. Recently, researchers have made advances in the development of clinical PAI systems that have deeper imaging depth, wider field of view and faster scanning times. This review describes the mechanics of PAI, some of its current biomedical applications and obstacles to clinical integration.

Keywords: *Photoacoustic Imaging, Non-Ionizing Imaging, Sound Waves*

1. Introduction

Photoacoustic imaging (PAI) is a relatively new imaging modality that derives its contrast from the optical absorption properties of tissue and biological cells. PAI depends on the propagation of energy into tissue, the interaction of this energy with the tissue, and the reception of produced acoustic energy [2,6]. Illuminating pulses are produced by a laser and absorbed by tissue. The absorbed energy gets converted into heat, whereupon rapid thermal expansion occurs and causes emission of an acoustic pressure wave [6]. This results in acoustic signals that are then wideband and detected by an ultrasonic transducer. Image reconstruction can then be utilized to produce two-dimensional (2D) images or three-dimensional (3D) tomographic images depending on the scan parameters [3,6].

PAI exploits the fact that every biological cell and tissue has a different optical absorption coefficient to create images. Also, because of this property different wavelengths can be used to image different parts of the body. The resolution for the resulting images are usually higher than that of other pure optical imaging modalities [11]. Furthermore, an image reconstruction algorithm can then be used to reconstruct a photoacoustic image in a configuration called photoacoustic computed tomography (PACT) [5,11]. PACT is a major configuration of PAI and Table 1 provides a list of commercially available PACT systems.

Although the technology has advanced in recent years, PAI is still far from being fully adopted into the clinical setting. Especially because already established imaging modalities such as computed tomography, and magnetic resonance imaging have long been the preferred method of imaging. Nonetheless, this review will summarize the literature regarding advances in PAI technology, and the hurdles it must overcome to be successfully integrated to the medical field.

Table 1. List of commercially available photoacoustic computed tomography (PACT) systems [5].

PACT system	Company	Cost	Image	Application
Vevo LAZR X	Fujifilm	~950K		Oncology, cardiology, molecular and neuro biology
Vevo LAZR	Fujifilm	~750K		Oncology, cardiology, molecular and neuro biology
PAFT	PST	~315K		Small animal imaging
MSOT inVision 128	iTheraMedical	~470K		Real-time whole body imaging
Nexus 128+	Endra Life	~375K		Molecular, tumor hypoxia, etc.
LOUISA 3D	TomoWave	~215K		Breast cancer

1.1 History

The beginnings of PAI can be traced to the 19th century when Alexander Graham Bell discovered the photoacoustic effect by observing that sound was

generated by the absorption of modulated sunlight [1,5]. However, it was not until the early 20th century that PAI began to be researched for medical applications. This was mostly due to the advances in laser light sources and acoustic detection equipment [6]. Figure 1 is a time graph of major events in the development of PAI.
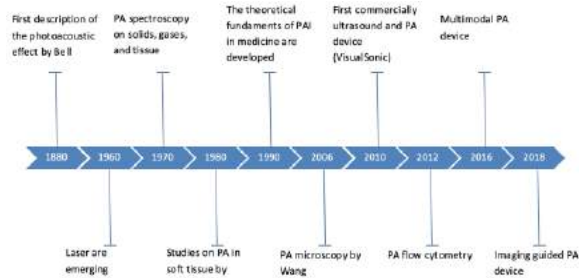

Figure 1. The history of photoacoustic imaging. Several decades passed from Bell's first description of the photoacoustic effect to the development of clinical applications [6].

1.2 Need for better imaging systems

Medical imaging is a vital tool for clinicians to diagnose and treat illnesses. Advancements in technology have yield better and more precise imaging modalities. However, as imaging technologies and general medical knowledge improve, more challenging targets are put before operators to intervene on [8]. The common practice of "expectant observation" is no longer sufficient to physicians as more and more of the previously "impossible to treat" lesions are within reach of operators [8,11].

According to *Wilt et al.* the chances of women having a false positive result after 1 mammogram ranges from 7-12 percent, depending on age [10]. Mammograms have undoubtedly reduced the prevalence or at least increase early detection of breast cancer. The X-ray based modality is far from perfect with about 87 percent sensitivity [10]. The adverse effects of a false-positive on women are highly severe and can have serious repercussions. That is why researchers agree that there is a need for better medical imaging modalities to replace or complement tests like mammograms.

The medical applications of PAI go beyond just detecting breast cancer and new applications continue to emerge. PAI, particularly PACT, are a suitable alternative to some of the already established imaging modalities.

2. Principle of PAI

The process of PAI requires a short pulse laser being illuminated onto the target tissue. The light beam then travels down the tissue and is absorbed by the soft tissue. The absorbed light energy causes localized heating, and the tissue then experiences thermoelastic expansion where it heats up and expands [2-6]. The temperature rise produces an initial pressure increase followed by relaxation, generating broadband low-amplitude ultrasound waves [6]. These ultrasound waves, also known as photoacoustic waves, are emitted from the target and can be captured by ultrasound transducers in different configurations depending the mode of imaging to produce a sequence of A-line signals [2,6]. An A-line signal is the display of the time-dependent response of the transducer generated by the ultrasound wave [6]. The A-line signals are then processed and combined to produce 2D photoacoustic images of the targeted tissue [2,6]. Figure 2 shows the typical setup for a PAI system and the order of events that lead to the image.
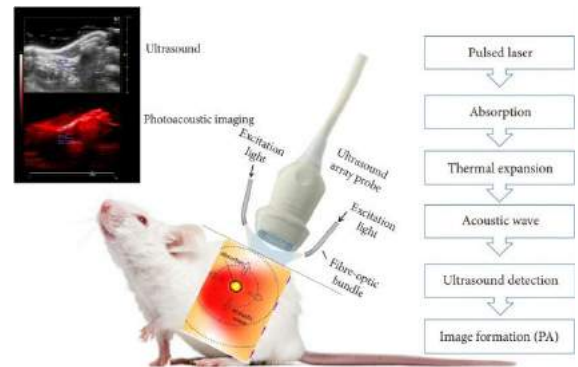

Figure 2. The basic principle of photoacoustic imaging. When a tissue is exposed to pulsed near-infrared laser light, the constituents of the tissue absorb light and undergo thermoelastic expansion, thereby causing ultrasound signals to emanate. These laser-induced ultrasound signals can be detected using an ultrasound transducer, making photoacoustic (or optoacoustic) imaging possible [6].

2.1 Instrumentation

While there is more than one setup, most PAI systems consist of a pulsed laser, an ultrasound transducer that detects signals emitted by the targeted tissue, and a data acquisition and display unit [4]. The pulsed nanosecond laser responsible for tissue irradiation in PAI typically operates in the visible or NIR wavelength range. The specific laser technology used is application specific; hence why clinical photoacoustic imaging systems are often region-specific. The systems utilize different laser-detector configurations for different applications because

37

biological absorbers (water, lipids, collagen, hemoglobin, etc.) can be targeted by irradiating tissue at the corresponding dominant absorption wavelength [6,11]. A tunable laser can be used to irradiate the tissue at wavelengths of interest in order to acquire multiple photoacoustic images that can be spectrally resolved for tissue composition to be assessed based on endogenous contrast [6,11].

Similarly, most clinical PAI systems use array transducers with multi-channel data acquisition systems [3]. The linear array transducer of ultrasound imaging is the most standard form of the PAI probes used, but curved, convex or concave can also be used [3,4]. Usually, non-linear transducers are used in order to increase the field-of-view. In particular, concave array transducers are used in order to provide better signal-to-noise ratio (SNR) and better visibility of large-size vessels compared to linear array transducers [4]. For example, a low-frequency handheld transducer array is best suited for imaging internal abdominal organs, and a high-frequency transducer is most desirable for superficial organs such as the skin and thyroid [7,11]. Therefore, the transducer utilized in a given PAI setup is determined by the application.

2.2 Image Reconstruction

For PAI, image reconstruction is done by processing the acoustic radio-frequency signals that are detected from the tissue. Although similar to ultrasound image processing, PAI's time-of-flight is short (about half) than for ultrasound because there is no backscattering [1,8]. As a result, received photoacoustic (PA) signals cannot be characterized by conventional pulse-echo speckle statistics [1,8]. Instead, because the acoustic generation resulting from the PA effect is omnidirectional, it is possible to operate PAI in either backward or forward modes [1,8,11].

The backward-mode, also known as reflection mode, utilizes a laser source and receiver that are in the same direction (coincident). Forward-mode, or transmission mode as is also called, relies on a receive transducer positioned such that it is sensitive to acoustic energy traveling away from the irradiation source. With backward-mode, one is able to generate A-line, B-mode, C-scan, or volumetric PA images [1,8]. Backward-mode PAI can be achieved with conventional delay-and-sum beamforming and can integrate ultrasound-based adaptive beamforming techniques [8]. This mode can be used for real-time imaging, catheter-based and endoscopic imaging, and PA microscopy [8].

The ability of PAI to implement forward-mode imaging is one of the major features that sets it apart from conventional ultrasound. Forward-mode PAI relies on an array of ultrasonic transducers to implement a computed tomographic (CT) imaging reconstruction [1,8,9,11]. Reconstruction of PA CT scans requires filtered back projection or inverse Randon transforms like with X-ray CT scans [1,11]. A more in depth mathematical description of reconstruction approaches for PAI is provided by Zhou and Yao [11].

Furthermore, PAI's spatial resolution and penetration depth correlate with the frequency of the emanated ultrasound [6,8]. As a result, a high ultrasound frequency of the PA signal results in better spatial resolution because the relative value decreases [6]. The maximum penetration depth simultaneously decreases as well, because higher ultrasonic frequencies are more attenuated than lower frequencies [6,8]. Hence, there is a trade-off between resolution and penetration depth as can be observed in formula 1.

$$\text{Relative Spatial Resolution} = \frac{\text{Penetration Depth}}{\text{Resolution}} \quad (1)$$

In general, PAI provides comparable resolution to that achieved with diagnostic ultrasound. Similar to ultrasound imaging, PAI's lateral resolution improves with an increase in the numerical aperture of the receiving array [1]. An increase in the array's center frequency and bandwidth increases resolution at the cost of decreased imaging depth [1,3]. This results in axial resolutions that range from 210 μm to 30 μm for transducer center frequencies ranging from 3.5 MHz to 20 MHz [3,7]. Although, in the case of PA microscopy, for which optical scattering is insignificant, lateral resolution can be as low as 220 nm because it is limited by the laser spot size [3].

3. Current applications

PAI is most beneficial for imaging in areas where differences in optical absorption exist. These differences in contrast occur naturally or due to use of an exogenous contrast agent [9]. Figure 3 shows optical absorption for different tissue types (a) and some exogenous contrast agents (b). The tunable peaks in part (b) of figure 3 shows that nanoparticles can be used as contrast agents in various applications [9].
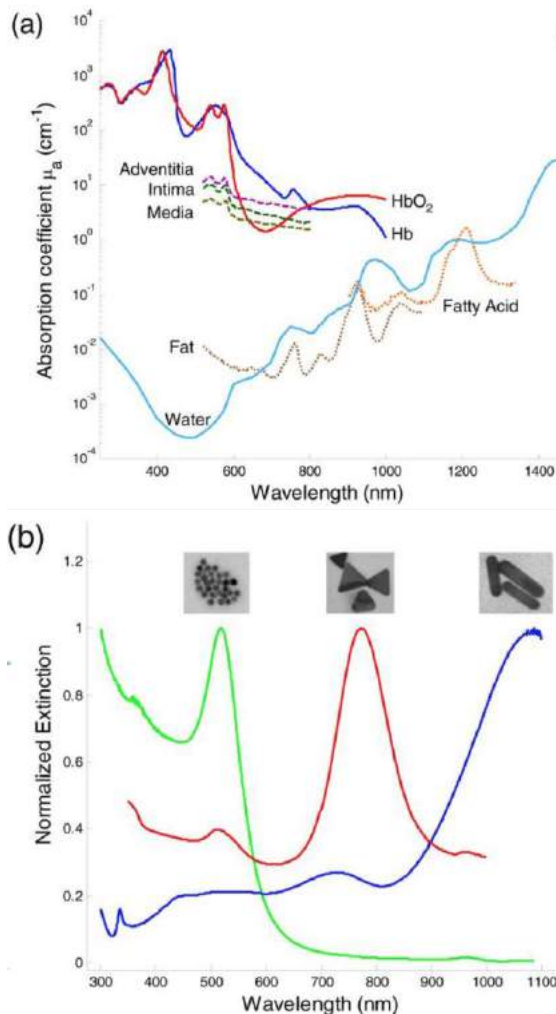
Figure 3. (a) Optical absorption spectrum of different tissue types which could be used as endogenous contrast agents in vivo. (b) Exogenous contrast agents such as gold nanospheres (16 nm diameter), silver nanotriangles (200 nm on edge), and gold nanorods (10 nm by 40 nm) and their corresponding extinction spectrum [9].

Because of its potential to utilize endogenous contrast agents, the number of clinical applications for PAI are ample. PAI can be used for diagnostic imaging, image-guided therapy and several other types of medical imaging.

3.1 Imaging-guided surgery

One of the most promising areas for clinical use of PAI is imaging-guided surgery (IGS). IGS refers to real-time correlation of the operative field with preoperative imaging data to determine the precise location of a selected surgical instrument relative to the surrounding anatomic structures [6].

The capability of PAI to provide imaging in real time make it an ideal candidate for IGS. Currently, surgeons are performing surgeries with static reference images (e.g., magnetic resonance images and computed tomography scans) of internal structures for guidance during surgical procedures. The novelty of having real-time images during surgery and utilizing PAI for locating structures is of great interest. Multiple researchers are investigating the use of PAI for minimally invasive IGS and in conjunction with other surgical devices such as robotic arms [6,11]. While further research is required for PAI to be widely used for IGS its potential suggest that eventually it will be commonly utilized in surgical procedures.

3.2 Cancer detection

Several studies have explored PAI as a tool for cancer detection, screening for tumor metastasis, and assessing tumor margins. The most researched type of cancer being breast cancer [2,10]. Some researchers consider PAI a possible alternative to X-ray mammography [1,6]. PA mammography requires a forward-mode system that facilitates 3-dimensional imaging of the patient's breast.

Similarly, PAI can be used to screen for metastasis using an exogenous agent [6]. Early-stage metastasis tends to occur in sentinel lymph nodes (SNL), which comprise a tumor bed that receives lymphatic drainage from cancerous tissues [1,6]. PAI has been shown to be able to detect SNL within tissue through the usage of an exogenous contrast [6]. In addition, researchers have used PAI to study prostate cancer in vivo using animal models and ex vivo ovarian imaging [3,6]. The applications of PAI for cancer studying are vast and more and more applications continue to emerge as the technology continues to advance.

3.4 Other biomedical applications

The applications for PAI are extensive and include but are not limited to: tissue engineering, drug delivery, cell biology, and functional brain mapping [2,3]. As the technology continues to capture the attention of research groups and companies, more and more biomedical applications emerge. Table 2 summarizes some of the recent applications of PAI.

Table 2. Summary of some of the medical applications for PAI [1].

Type of imaging	Applications
Anatomical imaging	• breast, pancreatic, colon, brain, and other cancer types imaging
Functional imaging	• oxygenation state and local concentration of hemoglobin • assessing local cerebral ischemia, anemia
Cellular/molecular imaging	• Tumor cell overexpression of contrast agents
Therapy mediation and monitoring	• Photothermal ablation • Photoactive drug release

4. Major challenges of PAI

Although PAI has several characteristics that make it a suitable candidate for clinical images there are aspects of the technology that still need to be addressed before it is widely integrated into the clinical setting. The desirable features of clinical PAI systems are deeper imaging depth, wider field of view (FOV), lower price, and faster scan time than those currently available [11].

4.1 Imaging depth

In order to achieve deep tissue penetration, near-infrared pulsed lasers with wavelength from 650 to 1100 nm are most commonly used [9,11]. These pulsed lasers maximize signal-to-noise ratio (SNR) in deep tissue with low extension [3,9]. High power pulsed lasers are also used to obtain high SNR in deep and wide areas. However, high-power pulsed lasers have a low frame rate and can be very expensive and bulky [9]. This has led researchers to utilize low power, less expensive compact laser diodes and light emitting diodes (LEDs) as a source of excitation [3,11]. These allow for a signal to be acquired multiple times and averaged in order to improve the SNR [3]. Yet, many believe that PAI will never provide image depth as deep as ultrasound (~10cm), which is why a lot more research is needed.

4.2 Field of view

Most PAI system are based off ultrasound and utilize a linear array transducer. However, this type of transducer limits the FOV of PAI [3]. Instead, clinical

PAI systems utilize array transducers with multi-channel data acquisition systems and different probe geometries. Several studies have looked at utilizing curved, convex or concave array transducers to increase FOV [3,7]. Compared to conventional linear array transducers, concave array transducers have better SNR and better visibility of large-size vessels [3]. Moreover, volumetric array transducers are used in PAI for acquiring three-dimensional (3D) and four-dimensional data [11]. This is what allows PAI form tomography images similar to those created by X-ray CT. Hence, the reason for vast amount of research devoted to the development of different probe configurations and geometries.

4.3 Contrast agents

PAI depends on the intrinsic optical absorption property of tissue constituents to differentiate tissue types and create images. As a result, researchers have developed exogenous contrast agents that can produce PA contrast with several fold higher magnitude than intrinsic endogenous contrast alone [9]. The most well-known contrast agents for PAI are plasmonic metal nanoparticles primarily made from gold and silver [6,9]. Plasmonic nanoparticles make for a good contrast agent because of its ability to under local surface plasmon resonance. This resonance is caused by oscillating electrons on the surface of the nanoparticles, which results in high attenuation of the incident electromagnetic wave [9]. The optical absorption of plasmonic nanoparticles can be increased by shape/composition modifications that include nanospheres, nanorods and nanocages [1,5,9]. Figure 3 shows the corresponding extinction spectrum for gold nanospheres, silver nanotriangles, and gold nanorods.

In addition to nanoparticles, there are other categories of exogenous contrast agents. For example, organic dyes are known to have distinct absorption properties and fluorescent proteins can also be used as contrast [9]. However, most research regarding PAI contrast in in relevance to nanoparticles. Many studies have looked at the toxicity, immunogenicity, and thermal increase of nanoparticles [4,7,11]. All studies concurred that further studies are needed before these contrast agents can be safely integrated into modern medicine practices.

4.4 Cost

One of the major factors keeping healthcare facilities from integrating PAI systems into their practice is cost. Of all of the components of PAI, the light source is by far the most expensive. Pulsed lasers are generally large and considerably expensive [4]. As such, researchers and companies have developed PAI systems that use low power, compact laser diodes and light emitting diodes (LEDs) as the source of excitation [3,11]. However, these modifications come with limitations such as lower SNR PA signals which consequently degrade the quality of the reconstructed images [3]. Nonetheless, researchers hope that these recent modifications to PAI systems will encourage more clinicians to utilize PAI.

Another major pricy component of a PAI system is the detection unit. As such, most PAI systems use already existing ultrasound detection systems and are typically integrated to clinically approved ultrasound equipment. This reduces the cost of creating new and specific detection system for PAI [5]. As mentioned before, this can consist of commercially available multiple single-element transducers or linear arrays. The limitations of these transducer arrays is where mechanically moving the transducer is not possible or high temporal resolution is required [3,5].

Lastly, the data acquisition component of the system is another major cost of PAI. Researchers believe that is mostly due to the lack of research in PAI. For example, *Han et al.* proposes using a very high sampling frequency data acquisition and multiplexing hardware/software can produce a low-cost data acquisition system [5]. However, more propositions similar to Han's are necessary before the development of proper low cost software can hit the market and be available for healthcare facilitates,

5. Discussion

PAI is a relatively new and developing field that has gained a large amount of attention in recent years. The ability to image differences in optical absorption in tissue make it a candidate for the detection of cancer, imaging-guided surgery, tissue engineering, and many others. Its success in preclinical studies offers promising results for clinical integration. However, successful clinical use of PAI is dependent on deeper light penetration depths typical of clinical procedures as well as regulatory concerns about the use of contrast agents in humans [1]. Targeted nanoparticle contrast agents, which have been shown to provide molecular specificity, sensing abilities, and signal enhancement

in small animal models, can be used to alleviate depth concerns and provide real-time cellular/molecular imaging [1,4]. Yet, concerns with their effectives, systemic clearance and toxicity have kept these agents from FDA approval and require further research.

Despite the concerns and limitations of PAI, the diagnostic and therapeutic potential of clinical PAI is significant. PAI systems, particularly those based on already established US systems, could integrate quickly into clinical practice. As the technology continues to improve and contrast agents to be developed, PAI could possibly be within reach of clinicians in a matter of years.

6. Conclusion

Photoacoustic imaging (PAI) is a promising modality with great potential for cancer detection, image-guided surgery, cellular/molecular imaging and countless other biomedical applications. This review explored the fundamental concepts of PAI, some of its current clinical applications, and some of the major challenges of the technology. Although there are already researchers looking to overcome some of these challenges there is still a need for novel and long-term studies.

7. References

1. Bouchard, R., O. Sahin, and S. Emelianov. Ultrasound-guided photoacoustic imaging: current state and future development. *IEEE Transactions on Ultrasonics, Ferroelectrics and Frequency Control.* 61:450-66, 2014.

2. Chan, J., Z. Zheng, K. Bell, M Le, P.H. Reza, and J.T.W. Yeow. Photoacoustic Imaging with Capacitive Micromachined Ultrasound Transducers: Principles and Developments. *Sensors.* 19:3617, 2019.

3. Choi, W., E.Y. Park, S. Jeon, and C. Kim. Clinical photoacoustic imaging platforms. *Biomedical Engineering Letters.* 8:139-155, 2018.

4. Erfanzadeh, M. and Q. Zhu. Photoacoustic imaging with low-cost sources; A review. *Photoacoustics.* 14:1-11, 2019.

5. Fatima, A., K. Kratkiewicz, R. Manwar, M. Zafar, R. Zhang, B. Huang, N. Dadashzadeh, J. Xia, and K. M. Avanaki. Review of cost reduction methods in photoacoustic computed tomography. *Photoacoustics.* 15:100137, 2019.

6. Han S.H. Review of Photoacoustic Imaging for Imaging-Guided Spinal Surgery. *Neurospine.* 15:306-322, 2018.

7. Kim, C., T.N. Erpelding, L. Jankovic, M.D. Pashley, and L.V. Wang. Deeply penetrating in vivo photoacoustic imaging using a clinical ultrasound array system. *Biomedical Optics Express.* 1:278-284, 2010.

8. Maybody, M., C. Stevenson, and S.B. Solomon. Overview of navigation systems in image-guided interventions. *Techniques in Vascular and Interventional Radiology.* 16:136-143, 2013.

9. Su, J.L., B. Wang, K.E. Wilson, C.L. Bayer, Y.S. Chen, S. Kim, K. A. Homan, and S.Y. Emelianov. Advances in Clinical and Biomedical Applications of Photoacoustic Imaging. *Expert Opinion on Medical Diagnostics.* 4:497-510, 2010.

10. Wilt, T.J., R.P. Harris, and A. Qassem. Screening for cancer: advice for high-value care from the American College of Physicians. *Annals of Internal Medicine.* 162:718-725, 2015.

11. Zhou, Y., J. Yao, and L.V. Wang. Tutorial on photoacoustic tomography. *Journal of Biomedical Optics.* 21:61007, 2016.

Mission Statement and Bylaws - Spring 2016

Mission

The mission of the journal is to develop the art of scientific writing among bioengineering students. Students may submit articles that describe original research or that review existing research (with proper credit listed in the references) that has been published elsewhere. Students may also submit papers that have been submitted for a grade in a UIC class. The journal also provides an opportunity for all bioengineering students to be involved as editors and reviewers. Thus, working on the publication of the journal will provide students with an overall appreciation of the processes involved in submitting, editing, and disseminating scientific findings. Additionally, through the publication of each issue, the journal serves to expose the authors, reviewers, and readers to current trends in the bioengineering field.

Scope

Submissions can range from original research articles and technical reviews to book or software reviews relevant to bioengineering. Letters to the editor are also welcome. Completed research projects are not necessary for publication. It is expected that some of the articles that appear in the journal will later be expanded into full-length studies and published elsewhere. Publication in the BSJ does not preclude later publication of the results in a copyrighted technical journal.

Bylaw

1. Editorial Board

   The BSJ shall elect one Chief Editor, one Editor-Elect, and one or more Associate Editors during the final week of classes. Editors shall be elected based on a vote of the current editorial board, reviewers, and authors. Editors must have at least one semester of experience participating in the journal, and must display qualities desired of an Editor such as active participation and timely completion of deadlines, and the Chief Editor must have held the position of Editor for at least one semester. When a new Chief Editor is chosen, they shall receive control of the BSJ Google Drive folder. The Editor-Elect shall continue in the position of the editor in the following semester. If the performance of the Editor-Elect is deemed unsatisfactory, including such factors as level of participation and interpersonal skills, the rest of the editorial board may choose a different editor to be Chief Editor the following semester. It is the responsibility of the Chief Editor to keep in regular contact with the Faculty Advisor and Department head about developments in the journal as well as update and maintain the Google Drive folder. Questions and concerns should be brought to the attention of the Faculty Advisor before anyone else. Finished journals and any funds raised should be sent to Jay Lin (jlin13@uic.edu).

2. Meetings

   The BSJ shall have general body meetings, to be held throughout the semester. One meeting must be held within the first two weeks of the semester, and at least once monthly afterwards. Meetings should introduce the journal to interested students and update members on paper statuses. Meeting times are to be finalized during the third week of school between 1:00pm-6:00pm on a day when the highest possible amount of board members can attend.

43

3. <u>Articles</u>

   Papers must follow the BSJ article template, available on Blackboard and the Google Drive folder. Content may include original research, technical reviews, book reviews, or software reviews. Other subjects may be allowed on a case-by-case basis. In the event that a paper authored by more than one student is submitted, names shall be listed in alphabetical order and each student must be involved in the review process. Papers shall be limited to two authors. No member may be the author of more than one paper per publication.

4. <u>Membership</u>

   Only bioengineering students may participate in the BSJ. In the event that a student from another major submits a paper, it shall be accepted on a case-by-case basis, depending on the quality of the paper and the number of previously submitted papers. To become a member, either as a reviewer or an author, interested students may email any of the editors, or the BSJ email account (bioejour@uic.edu).

TITLE OF THE ARTICLE

Author Name

e-mail

Abstract

The title should be 14pt, bold, Times New Roman all capitals. The author name must be in 12pt, Times New Roman, and email in 11pt Italics Times New Roman The abstract should be displayed in a 10pt, italic, Times New Roman font, justified, single column, with an additional left and right indentation of half an inch from the margin. Limit abstract to 300 words.

Keywords: *Template, UIC, Bioengineering, Student, Journal*

1. Introduction

This document represents the format for submissions to the student journal. The two-column format is followed for the body of the article. Text font should be 10pt Times New Roman, justified, single-spaced.

A single empty line should separate paragraphs, the end and beginning of different sections, and must be inserted above and below figures, tables, and equations.

2. Example of Numbered Heading

Each heading must be numbered and be in 12 point, bold, Times New Roman font, with the first letter of all words capitalized except for prepositions and conjunctions.
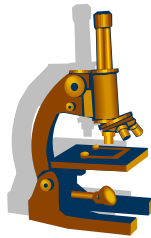

Figure 1. Figure captions are to be below the figure in 9pt Times New Roman, Justified

2.1 Example of Subheading and Table

Subheading must be in 11pt, bold, Times New Roman. Tables should be numbered in the order they appear.

Table 1. This table descriptor is 9pt Times New Roman, Justified

Column 1	Column 2	Column 3	Column 4
Row 1	This	is	Times
Row 2	New	Roman	10pt

3. Equation

Equations should be centered on separate lines with a single space above and below. The equation number should be indicated in parentheses at the rightmost of the last line of the equation.

$$E_{(a-t)} = m*a(s-h) + P_o + A(t)^o * \Sigma(s) \qquad (1)$$

4. Page Limit

Maintain a page limit of 5-10 pages for your entire submission.

List and number all references in 10-pt Times New Roman, single-spaced, at the end of your paper. When referenced in the text, enclose the citation number in square brackets, for example [1]. For multiple references separate using comma(s) [2, 6]. Where appropriate, include the name(s) of editors of referenced books. Arrange all references in alphabetical order of the 'Last Name' as demonstrated in the examples below.

5. References

(Reference format from Annals of Biomedical Engineering)

1. Guccione, J. M., A. D. McCulloch, and L. K. Waldman. Passive material properties of intact ventricular myocardium determined from a cylindrical model. *J. Biomech. Eng. Trans. ASME* 113: 42-55, 1991

2. Rideout, V. C. Mathematical Computer Modeling of Physiological Systems. Prentice Hall, Englewood Cliffs, NJ, 261 p.p., 1991

RICHARD AND LOAN HILL DEPARTMENT OF BIOENGINEERING

COLLEGES OF ENGINEERING AND MEDICINE

UIC